1   # The Neuromusculoskeletal Modeling Pipeline: MATLAB-based Model

2   # Personalization and Treatment Optimization Functionality for OpenSim

3   Hammond, C.V., Williams, S.T., Vega, M.M., Ao, D., Li, G., Salati, R.M., Pariser, K.M., Shourijeh, M.S.,

4   Habib, A.W., Patten, C., and Fregly, B.J.

5   ## Abstract

6   Neuromusculoskeletal injuries including osteoarthritis, stroke, spinal cord injury, and traumatic brain

7   injury affect roughly 19% of the U.S. adult population. Standardized interventions have produced

8   suboptimal functional outcomes due to the unique treatment needs of each patient. Strides have been

9   made to utilize computational models to develop personalized treatments, but researchers and

10   clinicians have yet to cross the "valley of death" between fundamental research and clinical usefulness.

11   This article introduces the Neuromusculoskeletal Modeling (NMSM) Pipeline, two MATLAB-based

12   toolsets that add Model Personalization and Treatment Optimization functionality to OpenSim. The two

13   toolsets facilitate computational design of individualized treatments for neuromusculoskeletal

14   impairments through the use of personalized neuromusculoskeletal models and predictive simulation.

15   The Model Personalization toolset contains four tools for personalizing 1) joint structure models, 2)

16   muscle-tendon models, 3) neural control models, and 4) foot-ground contact models. The Treatment

17   Optimization toolset contains three tools for predicting and optimizing a patient's functional outcome

18   for different treatment options using a patient's personalized neuromusculoskeletal model with direct

19   collocation optimal control methods. Support for user-defined cost functions and model modification

20   functions facilitate simulation of a vast number of possible treatments.

21   An NMSM Pipeline use case is presented for an individual post-stroke with impaired walking

22   function, where the goal was to predict how the subject's neural control could be changed to improve

23   walking speed without increasing metabolic cost. First the Model Personalization toolset was used to

24   develop a personalized neuromusculoskeletal model of the subject starting from a generic OpenSim full-

25   body model and experimental walking data (video motion capture, ground reaction, and

26   electromyography) collected from the subject at his self-selected speed. Next the Treatment

27   Optimization toolset was used with the personalized model to predict how the subject could recruit

28   existing muscle synergies more effectively to reduce muscle activation disparities between the paretic

29   and non-paretic legs. The software predicted that the subject could increase his walking speed by 60%

30   without increasing his metabolic cost per unit time by modifying existing muscle synergy recruitment.

31   This hypothetical treatment demonstrates how NMSM Pipeline tools could allow researchers working

32   collaboratively with clinicians to develop personalized neuromusculoskeletal models of individual

33   patients and to perform predictive simulations for the purpose of designing personalized treatments

34   that maximize a patient's post-treatment functional outcome.

35   # Abbreviations

36   NMSM Neuromusculoskeletal Modeling

37   JMP   Joint Model Personalization

38   MTP   Muscle-tendon Model Personalization

39   NCP   Neural Control Model Personalization

40   GCP   Ground Contact Model Personalization

41   TO   Tracking Optimization

42   VO   Verification Optimization

43   DO   Design Optimization

44   SynX   Synergy Extrapolation

45   IK   Inverse Kinematics

2

46 ID Inverse Dynamics

47 EMG Electromyography

48 DOF Degrees of Freedom

49 RMS Root Mean Squared

50 ADL Activity of Daily Living

51 TKR   Total Knee Replacement

52 CP Cerebral Palsy

53 GUI Graphical User Interface

54 XML Extensible Markup Language

1. Introduction

56 Approximately 19% of the U.S. adult population is afflicted by a movement impairment caused by

57 stroke, osteoarthritis, traumatic brain injury, limb amputation, cerebral palsy, Parkinson's disease, or

58 spinal cord injury.[1–3] In addition to the physical challenges caused by a movement impairment, these

59 individuals are more likely to experience increased health care costs, lower work productivity, a higher

60 risk of developing heart disease or diabetes, a reduction or loss of independence, and a decreased

61 quality of life.[1,4] At present, treatment of these life-altering impairments typically involves selection of a

62 standardized treatment based on subjective clinical assessment rather than design of a customized

63 treatment based on objective evidence-based methods. Consequently, existing treatments for

64 movement impairments do not address the unique clinical situation and needs of the individual patient

65 to the extent that they could, and should.

66 Not surprisingly, the standardized treatment paradigm is often unable to achieve the level of post-

67 treatment functional recovery that patients desire and expect. The percentage of patients who are

68 dissatisfied with their functional outcome following a standardized treatment supports this viewpoint.

69   For those who experience stroke, satisfaction with functional outcome is closely tied to ability to return

70   to a pre-stroke level of movement function.[5] However, stroke patient satisfaction with mobility

71   improvements generally declines after hospital discharge,[5] with only 65% of individuals post-stroke

72   recovering the ability to walk.[6] Even then, they tend to walk at a slow self-selected speed with an

73   asymmetric gait pattern that is less efficient metabolically than for healthy individuals.[6–8] Furthermore,

74   20% of stroke survivors remain dependent on others to perform activities of daily living (ADLs).[9] For

75   those with physician-diagnosed arthritis, roughly 44% have functional limitations that affect their ability

76   to perform ADLs.[10] For those who receive a total knee replacement (TKR), the best predictor of post-

77   surgery patient satisfaction is functional outcome.[11] However, 22% of TKR patients are dissatisfied with

78   their functional outcome one year after surgery,[12] while 16 to 30% are dissatisfied with their ability to

79   perform specific ADLs.[13] For those who receive a total hip replacement, 7% are dissatisfied with their

80   functional outcome,[14] with expectations for improved walking and stair climbing ability not being met in

81   over 30% of patients.[15] For those who receive opening wedge high tibial osteotomy surgery, 22% are

82   dissatisfied with their outcome, primarily due to unmet expectations for their post-surgery ability to

83   perform functional activities.[16] For those with cerebral palsy (CP), 33% do not improve walking speed as

84   a result of multi-level orthopedic surgery,[17] while 21% of parents of children with CP do not feel that

85   their child's orthopedic surgery was worth the time, effort, pain, and cost.[18] More than 50% of children

86   with CP who undo multi-level surgeries do not see improvements in their gait patterns[19]. For those with

87   lower limb amputation, between 12 and 32% cannot perform desired ADLs with their prosthesis, while

88   only 30% to 52% find the same ADLs very easy to perform.[20] Those with upper limb amputation use their

89   prosthesis primarily for cosmetic rather than functional reasons, with the percentage of individuals who

90   rate their upper extremity prosthesis as beneficial for performing various ADLs ranging from 5% to only

91   25%.[21] These statistics across a myriad of clinical conditions that impair movement highlight the need for

92   a better treatment design paradigm to help a larger percentage of patients recover their desired amount

93   of post-treatment function.

94   One possible way to improve treatment design and thus functional outcomes for individuals with

95   movement impairments is to employ engineering design optimization methods that utilize physics-

96   based computational models. Physics-based computational models have an advantage over "black box"

97   machine learning models since they extrapolate better to situations outside the boundaries of the

98   training data, which is where optimal solutions often lie. Engineering design optimization methods have

99   dramatically improved function and reliability of commercial products in numerous industries including

100   automotive, aerospace, farming, construction, and structural engineering, among others.[22–27] Using

101   these virtual prototyping methods, engineers can evaluate countless designs – including highly novel

102   ones – in a time- and cost-efficient manner to determine an optimal design for a given problem, thereby

103   reducing or eliminating trial-and-error design iterations performed on physical prototypes. Researchers

104   have already demonstrated the benefits of combining engineering design optimization with

105   personalized models to develop effective personalized interventions for a small number of clinical

106   problems.[28–33]

107   While a similar computational approach holds promise for designing personalized treatments for

108   movement impairments, at least three significant challenges must first be overcome for such an

109   approach to become a reality. First, researchers must be able to personalize the neuromusculoskeletal

110   computer models used in the computational treatment design process.[34] Published musculoskeletal

111   modeling studies have typically used scaled generic models rather than models whose relevant

112   characteristics have been personalized to a subject's movement data.[34] This decision is understandable

113   given the challenges of collecting the experimental movement (and possibly imaging) data needed for

114   the model personalization process coupled with the challenges of performing the personalization

115   process itself for any aspect of a model (e.g., joint functional axes). However, differences between

116   patients with the same clinical condition are precisely what make the clinical treatment design process

117   so challenging. Second, researchers must be able to perform the treatment design optimization process

118   using a patient's personalized neuromusculoskeletal model. Such a process requires performing

119   repeated predictive simulations of patient function following different implementations of a planned

120   intervention. To date, the majority of such simulations have been performed using "home brew"

121   computational software,[35–47] making it difficult for the broader research community to engage in the

122   process, to repeat studies performed by others, and to transfer knowledge about the process to others.

123   Third, researchers must have access to computational software that makes the model personalization

124   and treatment optimization processes easy, repeatable, and transferable. While recent software

125   advances such as OpenSim Moco[48] have made it possible to perform predictive simulations more easily,

126   neither OpenSim[49,50] nor Moco[48] provide means to personalize relevant aspects of a patient's

127   neuromusculoskeletal computer model or to use a personalized model to perform the treatment design

128   optimization process.

129   Several existing musculoskeletal modeling software tools have sought to address these challenges to

130   various degrees.[51–58] These tools primarily focus on personalizing the musculoskeletal model creation

131   process, including personalizing bone geometry from medical imaging data, personalizing muscle

132   attachment points on bones, and generating scaled generic musculoskeletal models using automated

133   methods. The SimCP simulation platform, designed to predict post-surgery walking function for

134   individuals with cerebral palsy, goes beyond other tools in several important ways.[51] It supports

135   personalization of Hill-type muscle-tendon model properties, personalization of neural control

136   properties using a muscle synergy structure, and prediction of the joint moment "capability gap" that

137   would remain following implementation of a proposed surgical plan. Nonetheless, none of these tools

138   can personalize multiple aspects of a patient's neuromusculoskeletal computer model and then use the

139   personalized model within a predictive simulation framework to design clinical interventions.

140   This article introduces the Neuromusculoskeletal Modeling (NMSM) Pipeline, a MATLAB-based

141   software package that provides researchers and clinicians working together with state-of-the-art

142   computational tools for designing effective personalized treatments for movement disorders. The

143   software package is built on the foundation of the OpenSim musculoskeletal modeling software and

144   adds two toolsets to OpenSim[49,50]. The Model Personalization toolset uses patient movement data and

145   gradient-based optimization to personalize four subcomponents of a patient's neuromusculoskeletal

146   computer model: 1) joint structure models, 2) muscle-tendon models, 3) neural control models, and 4)

147   foot-ground contact models. The Treatment Optimization toolset uses a patient's personalized model

148   with direct collocation optimal control methods[35,41,48,59–62] to predict how the patient's neural control

149   and/or anatomy should be changed, or how an external device (e.g., an exoskeleton) or implant should

150   be designed and/or controlled, to maximize improvement in the patient's post-treatment movement

151   function. By emphasizing functionality, ease of use, flexibility, and computational speed, the NMSM

152   Pipeline will hopefully accelerate involvement of the neuromusculoskeletal modeling research

153   community in the computational design of clinically implementable personalized neurorehabilitation

154   and surgical interventions.

155   The remainder of this article is outlined as follows. First, a design overview of the NMSM Pipeline is

156   presented, including an overview of the philosophy and goals of the software and an introduction to the

157   two included toolsets. Second, implementation details, design decisions, and important information for

158   each tool are presented. Third, an example treatment design use case is provided including specifics

159   about the use of each tool and final results. Fourth, a discussion section is included to provide

160   information about future work, limitations, and access to the software.

161   2. Design Overview

162   2.1 Philosophy and Goals

163   The goal of the NMSM Pipeline software is to help neuromusculoskeletal modeling researchers

164   engage in clinical research - and cross the valley of death,[63] thereby moving neuromusculoskeletal

165   modeling a significant step closer to becoming a clinically useful tool. To achieve this goal, the NMSM

166   Pipeline uses a personalized medicine approach, where physics- and physiology-based personalized

167   neuromusculoskeletal computer models constructed from patient movement data are used to design

168   personalized treatments for movement impairments.[64] Such impairments arise from clinical conditions

169   like osteoarthritis, stroke, cerebral palsy, spinal cord injury, Parkinson's disease, limb amputation, and

170   even cancer. Because the open-source OpenSim[49,50] and commercial Anybody[65] software commonly

171   used for musculoskeletal modeling research lack the ability to personalize neuromusculoskeletal

172   computer models to patient movement data, these software tools cannot currently be used to optimize

173   treatments for individual patients. To overcome this critical limitation, the open-source NMSM Pipeline

174   software uses MATLAB (The MathWorks, Natick MA) to build on the OpenSim foundation and provides

175   two new toolsets - a Model Personalization toolset that facilitates the creation of personalized

176   neuromusculoskeletal computer models, and a Treatment Optimization toolset that uses the

177   personalized models to design personalized treatments that maximize a patient's post-treatment

178   movement function.

179   To develop these two new MATLAB-based toolsets, we defined a high-level software design

180   philosophy. First, the NMSM Pipeline was designed to be both accessible for basic users and extensible

181   for advanced users so that neuromusculoskeletal modeling researchers of all levels can benefit from it.

182   Second, modeling and simulation methods were based on laws of physics and principles of physiology

183   and neuroscience rather than on machine learning, since no training data exist for post-treatment

184   movement conditions, and machine learning methods do not, in general, extrapolate well outside the

185   boundaries of the training data. Third, existing OpenSim functionality and model entities were utilized to

186   the fullest extent possible to avoid duplication. Fourth, NMSM Pipeline functionality was designed to

187   have the "look and feel" of OpenSim so that those with experience using OpenSim can quickly become

188   proficient using the Pipeline. Fifth, the NMSM Pipeline was designed to work with any OpenSim model,

189   providing complete flexibility in the musculoskeletal anatomy and movement situations that can be

190   modeled and simulated.

191   To achieve the goal of accessibility for basic users and extensibility for advanced users, we designed

192   NMSM Pipeline tools to work using Extensible Markup Language (XML) settings files, similar to OpenSim.

193   This approach allows users to run each NMSM Pipeline tool with only a single line of code. For basic

194   users, we developed two OpenSim GUI plugins - one for the Model Personalization toolset with its four

195   tools, and one for the Treatment Optimization toolset with its three tools, where each toolset appears

196   under the OpenSim "Tools" menu. The GUI plugin window for each tool allows users to set up tool runs

197   by configuring the most common settings for each tool (Figure 1), with default values being used

198   automatically for advanced tool settings. Tool settings selected in the GUI plugin, along with default

199   advanced tool settings, can be exported by

200
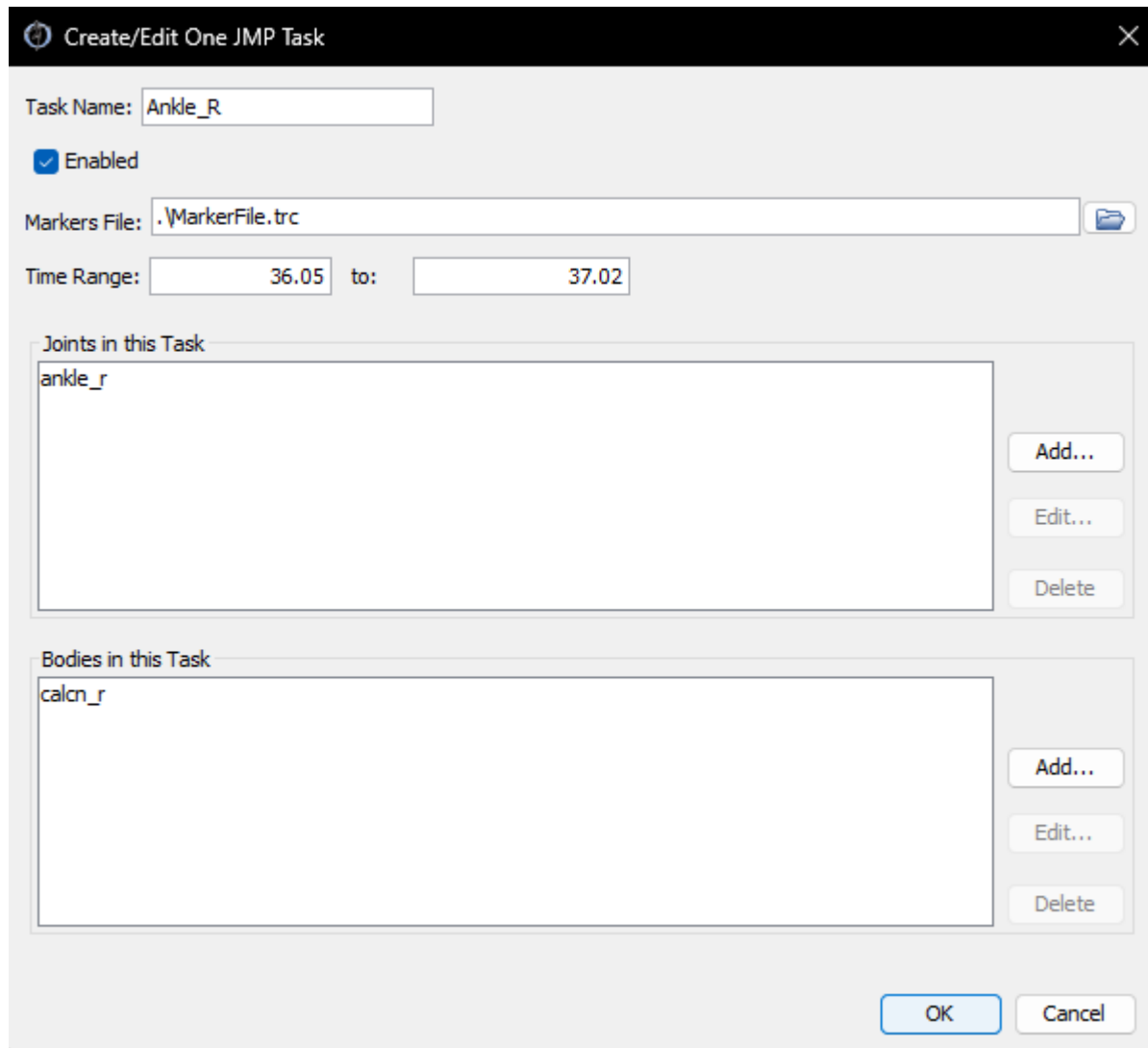
201   **Figure 1**: Screenshot of the JMP GUI tool sub-window for adding a JMP task. The GUI tools allow for

202   modifying common settings and creating XML settings files. Advanced settings can be modified directly

203   in the XML file after creation.

204

205   the user to an XML settings file that can be read back into the GUI and modified as desired, just as with

206   OpenSim tools. For advanced users, advanced tool settings are exposed in each tool's XML settings file,

207   again similar to OpenSim. Advanced users can create an initial XML settings file using the GUI plugin, or

208   they can start from a pre-existing XML settings file and edit the values of basic and advanced tool

209   settings using any text editor. For both basic and advanced users, each tool is run from the MATLAB

210   command line using a tool-specific function that takes a tool-specific XML settings file as an input. Thus,

211   no "Run" button is provided in any of the GUI plugin tool windows. Tool outputs can be plotted in

212   MATLAB using included utility or custom functions.

213   Software engineering principles were used for NMSM Pipeline development to facilitate

214   extensibility. Namely, atomic functions - functions that complete only a single operation - were used

215   extensively. All code was written using clear, English-language variable and function names and

216   organized into logical groupings. GitHub's source control, automated testing framework, and continuous

217   integration tools were used to maintain this extensive project and its documentation throughout the

218   development process. These choices make NMSM Pipeline code easy to understand and easy to modify.

219   Because NMSM Pipeline tools are based on laws of physics and principles of physiology and

220   neuroscience, we selected computational methods that best facilitate the intended personalized

221   medicine approach. Gradient-based optimization was used for all tools within the NMSM Pipeline

222   primarily for computational speed reasons but also for the ability of gradient-based optimizers to find

223   better solutions than the initial guess, even if the final solution is not the global optimum. For the Model

224   Personalization toolset, built-in MATLAB optimization algorithms (primarily lsqnonlin and fmincon) were

225   used exclusively, while for the Treatment Optimization toolset, the open-source IPOPT optimizer[66] was

226   used within the commercial GPOPS-II direct collocation optimal control software.[60] This approach

227   eliminates GPOPS-II and direct collocation optimal control from the Model Personalization process,

228   making model personalization a more reliable and less complex process than it would be if direct

229   collocation optimal control were required.[41,67,68] The Model Personalization toolset automatically uses

230   MATLAB's built-in parallel processing capabilities for calculating finite difference derivatives needed by

231   MATLAB optimization algorithms, while the Treatment Optimization toolset automatically uses parallel

232   processing only for repeated OpenSim analyses performed through MATLAB via C++ Mex files.

233   Through the utilization of OpenSim's native models and entities, we included a number of

234   convenient facilities in the NMSM Pipeline. OpenSim native file types were used for all data interactions

235   including OpenSim model files (.osim), marker data files (.trc), kinematic motion and ground reaction

236   data (.mot), time series data (.sto), and XML settings files (.xml). Only one new file type was developed--

237   the NMSM Pipeline model file type (.osimx) to store personalized model properties that are not included

238   in native OpenSim models. Similarly, easy-to-use OpenSim GUI tools such as the Scale tool, Inverse

239   Kinematics (IK) tool, Inverse Dynamics (ID) tool, and Muscle Analysis tool were leveraged as part of the

240   typical pipeline run-through using experimental movement data. For some NMSM Pipeline tools, groups

241   of muscles must be identified, and the muscle groups functionality available in OpenSim models was

242   used for this purpose to avoid the need to store this group information elsewhere.

243   ## 2.2 NMSM Pipeline Toolsets

244   The NMSM Pipeline is composed of two toolsets-- a Model Personalization toolset and a Treatment

245   Optimization toolset. The Model Personalization toolset personalizes four aspects of a scaled generic

246   OpenSim model using experimental movement data and gradient-based optimization (Figure 2). Those

247
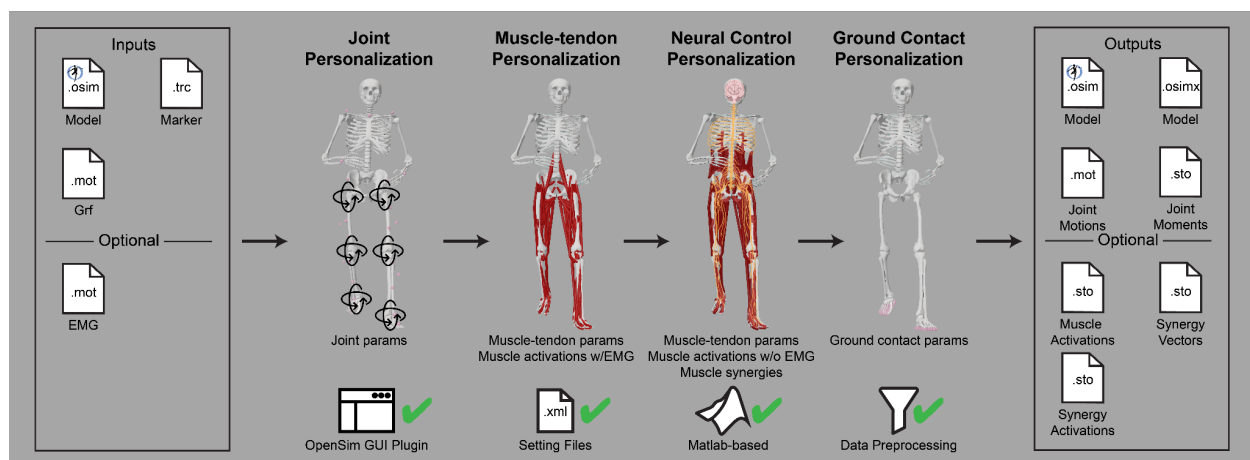
248　　　**Figure 2:** Overview of the Model Personalization toolset. This toolset creates neuromusculoskeletal

249　　models with personalized joint, muscle-tendon, neural control, and ground contact parameters through

250　　the use of gradient-based optimization.

251

252　　four aspects are 1) joint models, 2) muscle-tendon models, 3) neural control models, and 4) ground

253　　contact models. The personalization process is important since personalized rather than generic models

254　　are needed to support model-based treatment design for clinical conditions where patients exhibit

255　　significant heterogeneity (e.g., stroke).[69,70] Furthermore, without a personalization process,

256　　neuromusculoskeletal models do not reliably predict internal muscle and joint contact forces, body

257　　motion, or metabolic cost.[41,71–78] Each stage in the NMSM Pipeline Model Personalization process has

258　　been shown to play an important role in predicting these quantities reliably.[41,71–73,78,79]

259　　　　The Treatment Optimization toolset uses the subject's personalized neuromusculoskeletal model to

260　　predict their post-treatment movement function using direct collocation optimal control (Figure 3). Over
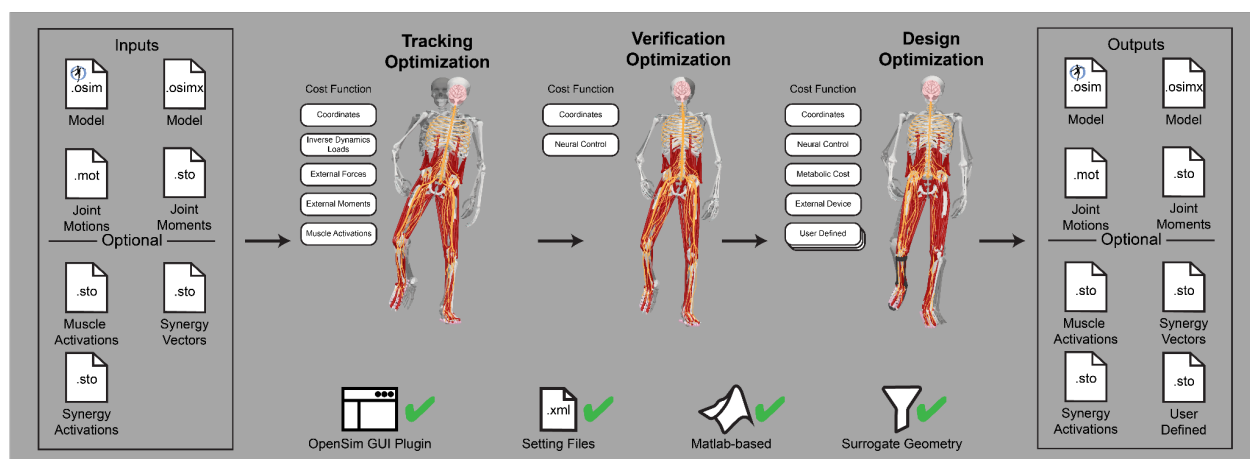

262　　　**Figure 3:** Overview of the Treatment Optimization toolset. This toolset generates a tracking

263　　simulation and two subsequent predictive simulations through the use of direct collocation optimal

264　　control.

265

266   the past 10 years, musculoskeletal modeling researchers have converged on direct collocation optimal

267   control as the best method for generating predictive simulations of human movement.[35–]

268   [37,37,40,41,48,59,67,80–88] The Treatment Optimization Toolset uses the MATLAB-based GPOPS-II direct

269   collocation optimal control software[60] to perform predictive simulations of movement for novel

270   conditions where no experimental data exist. Similar to MATLAB, GPOPS-II is inexpensive for academic

271   use. The optimal control solver can adjust neural and/or torque control signals along with neural

272   control, anatomical, internal implant, and/or external device parameters in a patient's personalized

273   neuromusculoskeletal model to achieve a specified treatment goal (e.g., achieve a desired reduction in

274   metabolic cost). For any patient, this approach can potentially provide the best treatment prescription,

275   the best dosage, and an estimate of the patient's capacity for improvement.

276   Optimization cost function terms for both toolsets were designed to minimize squared errors and/or

277   cost term values and utilize a common formulation with physically meaningful cost function parameters.

278   Specifically, cost function terms utilize a maximum allowable error and, in some cases, a user-provided

279   error center (Figure 4). For example, if a cost function term seeks to minimize errors between model and
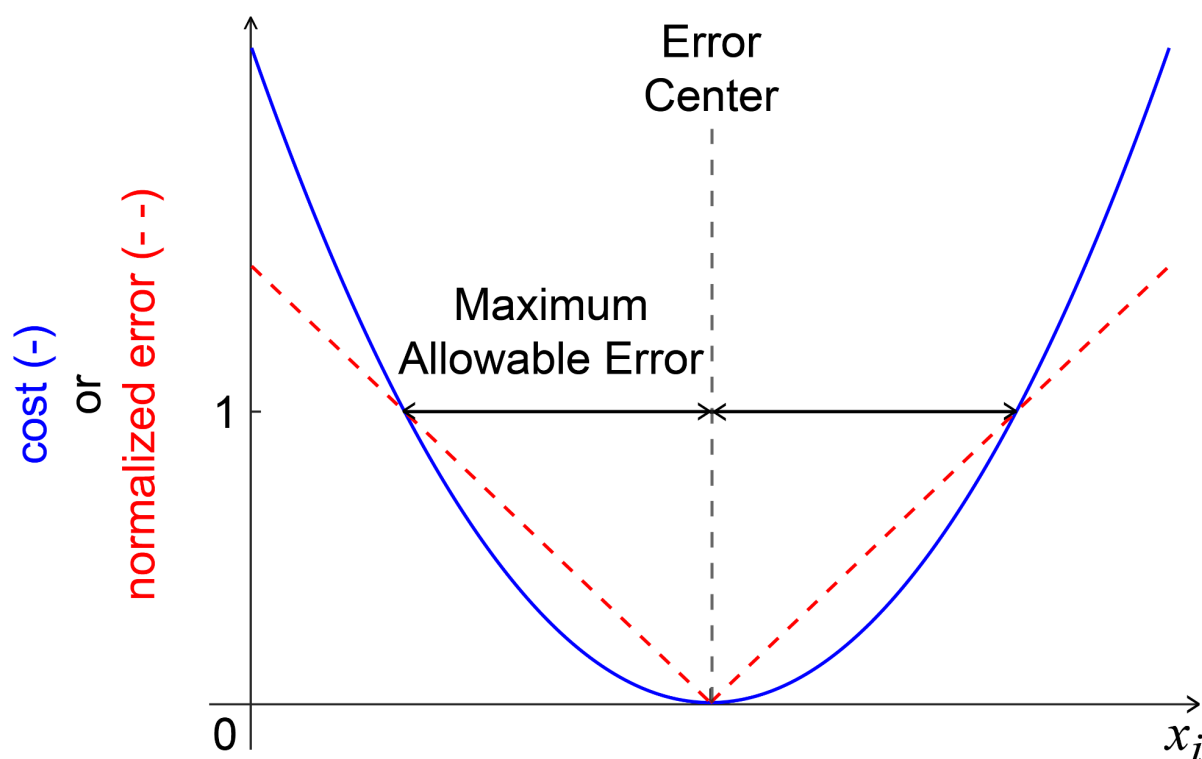
$$cost = \frac{1}{npts} \sum_{i=1}^{npts} \left(\frac{x_i - error\_center}{max\_allowable\_error} \right)^2$$

280

281 **Figure 4:** The generic cost function term formulation used throughout the Model Personalization

282 and Treatment Optimization toolsets. The formulation utilizes a maximum allowable error and error

283 center to make the calculated cost physically meaningful. If the difference between the current value

284 and the error center is greater than the maximum allowable error, then the quantity in parentheses will

285 be greater than 1, and squaring this quantity will amplify the cost (e.g., 1.1^2 = 1.21). In contrast, if the

286 difference between the current value and the error center is less than the maximum allowable errors,

287 then the quantity in parentheses will be less than 1, and squaring this quantity will attenuate the cost

288 (e.g., 0.9^2 = 0.81). Some cost function terms track experimental time-varying data, these have an

289 implicit error center of the experimental data value. Some cost function terms minimize errors relative

15

290   to a static reference value. The type of the cost function term is included in the name for Treatment

291   Optimization cost function terms.

292

293   experimental joint moments, and matching to within 2 Nm is acceptable, then the user would set their

294   cost term error center to 0 and the associated maximum allowable error to 2. Each cost function term

295   has equal weight with all other cost function terms included in the optimal control problem formulation,

296   where continuous cost function terms involving time series data (e.g., joint angles, joint moments) are

297   normalized by final time so that they do not contribute to the total cost more heavily than do terminal

298   cost function terms involving only a single quantity (e.g., metabolic cost). This method for formulating all

299   cost function terms allows for contextualized decision-making when determining weights for different

300   cost function terms.

301   Neural control models for both toolsets are described using muscle synergies. Muscle synergies

302   provide a physiologically-relevant low dimensional representation of a large number muscle activations

303   and can be personalized to represent a specific patient's neural control strategy.[89–97] Each muscle

304   synergy is composed of a time-varying synergy activation and an associated time-invariant synergy

305   vector. Each synergy vector contains a weight for each muscle in the model that defines how the

306   associated synergy activation contributes to the total activation of the muscle. Muscle synergies are

307   commonly calculated using non-negative matrix factorization,[89,90] and typically between three and six

308   muscle synergies are required to account for over 95% of the signal variability for common tasks such as

309   walking, running, and reaching.[98]

3. Implementation Details

3.1 Model Personalization

The Model Personalization toolset calibrates parameter values in an OpenSim neuromusculoskeletal model so that the model closely reproduces a wide range of experimental movement data. The toolset consists of four tools and was designed so that the tools can be used largely independently from one another, though a preferred tool workflow exists. Personalization is likely to be necessary if the musculoskeletal model is to be used for clinical treatment design purposes.[34] It also improves models for use in predictive simulations by maximizing the self-consistency of collected experimental data and easing the task of finding a realistic, dynamically consistent motion.

The four tools of the Model Personalization toolset personalize different anatomical, physiological, and neurological aspects of a patient's OpenSim model. Joint Model Personalization (JMP) calibrates the properties of OpenSim constraint-based joint models, Muscle-tendon Model Personalization (MTP) calibrates the properties of Hill-type muscle-tendon models, Neural Control Model Personalization (NCP) calibrates the properties of muscle synergy control models, and Ground Contact Model Personalization (GCP) calibrates the properties of elastic foundation foot-ground contact models. OpenSim models personalized using the Model Personalization toolset can be used in both the NMSM Pipeline's Treatment Optimization Toolset and, in the near future, OpenSim Moco. For use with OpenSim Moco, an NMSM Pipeline .osimx model file must be converted to an OpenSim .osim model file using an provided MATLAB model conversion utility program.

The Model Personalization toolset requires input data generated using standard OpenSim tools. First, a generic musculoskeletal model is scaled using the OpenSim Scale Model tool. To facilitate modeling and simulation of full-body walking motions, we recommend starting with the RCNL2023 OpenSim model (distributed with the NMSM Pipeline software), which is a modified version of the

333   Rajagopal full-body OpenSim model[99] where the ankle joint kinematic model has been changed to match

334   van den Bogert et al. (1994)[100] and the knee joint kinematic model changed to eliminate all rotational

335   offsets while producing the same motion. A scaled generic model is one of the required inputs for the

336   JMP tool. After the joints of the model are personalized to the individual's functional joint axes using the

337   JMP tool, the user must calculate IK motions and ID loads using the OpenSim Inverse Kinematics and

338   Inverse Dynamics tools, respectively. The user must then run the Muscle Analysis tool to calculate

339   muscle-tendon lengths and velocities as well as muscle moment arms if the NMSM Pipeline MTP and

340   NCP tools are to be used. For the JMP tool, marker files can be manually concatenated to personalize

341   joint parameters, values that characterise the transformation of the parent and child bodies of a joint,

342   using multiple motion trials (e.g., marker data from isolated ankle, knee, and hip motion trials can be

343   concatenated with marker data from a walking motion trial to calibrate the functional axes and joint

344   centers of all lower body joints simultaneously). The MTP and NCP tools accept data from one or more

345   motion trials, and the GCP tool accepts data from only a single motion trial, ideally the same trial to be

346   used for Treatment Optimization. If multiple motion trials are used with either the MTP or NCP tools, IK

347   motions, ID loads, muscle-tendon lengths and velocities, and muscle moment arms need to be

348   calculated for each motion trial.

349   3.1.1 Joint Model Personalization

350   The Joint Model Personalization tool optimizes joint parameters, body scaling, and marker

351   placement to minimize IK marker distance errors.[100–106]. Reducing inverse kinematics marker distance

352   errors reduces downstream errors in calculated inverse dynamic joint moments[72], muscle-tendon

353   lengths and velocities, muscle moment arms, and ultimately muscle activations and forces. These

354   quantities are used by subsequent Model Personalization tools.

355   JMP tool inputs are a scaled generic OpenSim model and marker data from one or more motion

356   trials, where the tool settings file allows the user to specify one or more tasks (Figure 5). The design

357
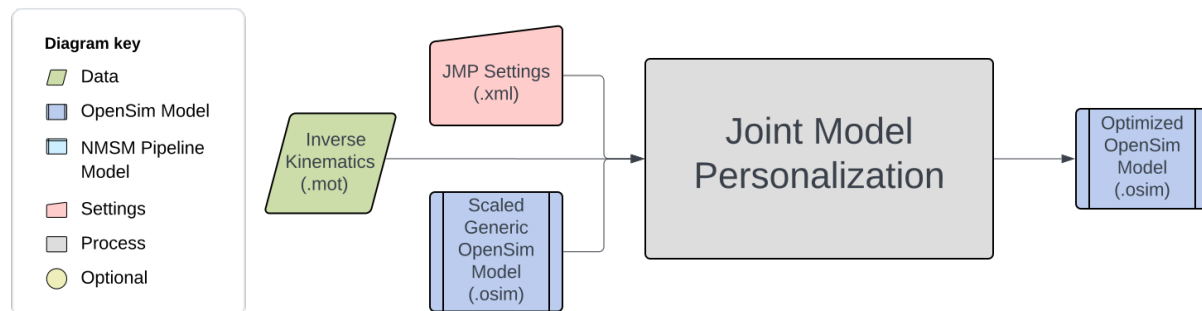
Figure 5: Flowchart showing the inputs to and outputs from the JMP tool. The diagram key also

359   applies to Figs. 6 through 9.

360

361   variables available in a JMP settings file include joint locations and orientations in parent and child

362   bodies, body scale factors applied uniformly, and marker location offsets for each direction

363   independently. The only cost function term is the sum of the squared marker distance errors normalized

364   by the motion trial duration and number of markers. No constraints are included in this optimization

365   problem. The output of JMP is a new OpenSim model with optimized joint parameters, body scale

366   factors, and/or marker placements.

367   Several important considerations should be kept in mind when using the JMP tool. A JMP run can be

368   split into multiple tasks, each with its own set of design variables and an associated marker file. Careful

369   JMP setup is required to avoid obtaining non-anatomical results. Such a result could be found by

370   personalizing a joint parameter for a coordinate that does not move through sufficient range of motion

371   (> ~25 degrees) during the motion trial[107]. This issue can be rectified by personalizing the associated

372   joint parameters with separate tasks using isolated joint motion trials, or by concatenating data from an

373   isolated joint trial with data from the desired functional trial (e.g., walking). Another cause of non-

374   anatomic results is selection of joint parameters that produce relative bone motions that are

19

375   inconsistent with joint function. For example, the parent frame of the hip joint is often defined to be at

376   the center of the acetabulum, while the child frame is often defined to be at the center of the femoral

377   head. Allowing joint parameters to modify the location of the hip joint in either the parent or the child

378   frame could move the center of the femoral head out of the center of the acetabulum, breaking that

379   anatomical relationship. In addition, muscle paths and/or relative body sizes may also become non-

380   anatomical due to inclusion of inappropriate design variables. JMP tool results should be visualized in

381   the OpenSim GUI and problem formulations modified to achieve an anatomically realistic post-JMP

382   model.

383   3.1.2 Muscle-tendon Model Personalization

384   The Muscle-tendon Model Personalization tool finds an optimal set of subject-specific muscle-

385   tendon properties and muscle activations from EMG, joint kinematic, and joint moment data by

386   balancing optimization cost function terms related to muscle properties, similarity of properties among

387   grouped muscles, and matching of EMG-driven and experimental inverse dynamics joint

388   moments.[75,76,108,109] Muscle activation and force predictions are sensitive to optimal muscle fiber length

389   and tendon slack length.[71,110–112] Therefore, reliable personalization of these parameters is essential for

390   generating reliable predictions of muscle activations and forces during predictive simulations of

391   movement.

392   The inputs to the MTP tool are a post-JMP OpenSim model as well as IK motion, ID load, muscle-

393   tendon length and velocity, and muscle moment arm data from one or more motion trials of interest

394   (Figure 6). The design variables that can be optimized include activation dynamics and muscle-tendon

395   length parameters for each muscle.[41,75,113] Cost function terms used by the MTP tool

396
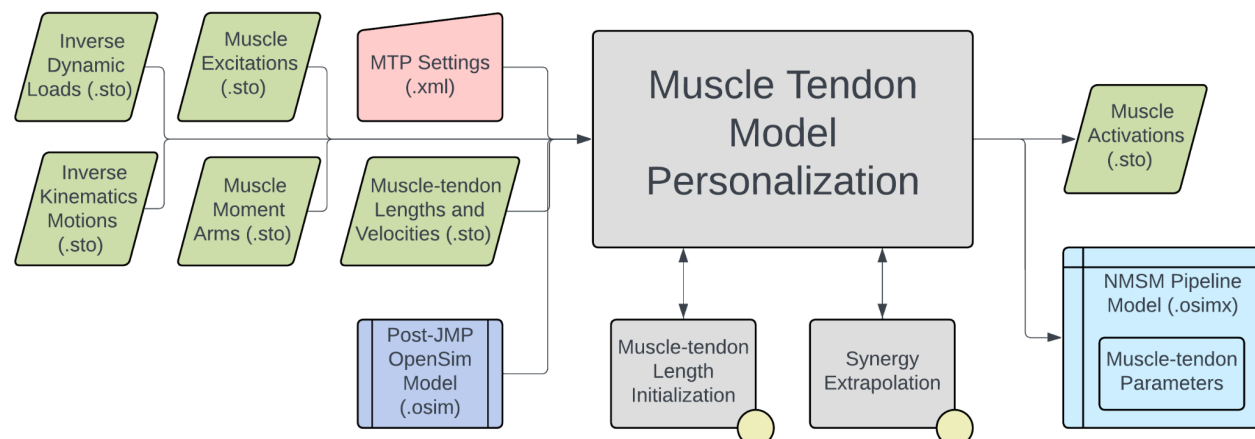
397   **Figure 6:** Flowchart showing the inputs to and outputs from the MTP tool. The diagram key is

398   included in Fig. 5.

399

400   minimize muscle-tendon model parameter deviations from initial values, ID joint moment tracking

401   errors, passive muscle forces, inconsistencies among grouped normalized muscle fiber lengths,

402   inconsistencies among grouped muscle excitation scale factors, and inconsistencies among grouped

403   electromechanical delays. No constraints are applied in this optimization problem. The outputs of the

404   MTP tool are a .osimx model file containing optimized muscle-tendon properties and estimated muscle

405   activations, both for use by other tools in the NMSM Pipeline.

406   Several important considerations should be kept in mind when using the MTP tool. Muscle Tendon

407   Length Initialization is included as an option within the MTP tool and is typically used to find initial

408   values for muscle-tendon length parameters that act as reasonable reference values for cost function

409   deviation terms involving muscle-tendon length parameters. Muscle Tendon Length Initialization also

410   estimates the maximum isometric force of each muscle based on published regression relationships.[114]

411   Since scaling maximum isometric force and muscle excitation at the same time produces a non-unique

412   muscle force solution, and since muscle excitations are scaled using EMG scale factor design variables,

413   maximum isometric force is held constant during an MTP tool run.[71] Synergy Extrapolation (SynX)[115,116] is

21

414   also included in the MTP tool to estimate the activations of muscles without experimental EMG data.

415   SynX uses muscle synergy concepts to estimate missing activations and is more accurate than

416   traditionally used static optimization at predicting missing EMG signals[117]. A typical use case for SynX is

417   estimating the activations of deep muscles from which EMG data cannot be easily collected. SynX can

418   use either principal component analysis or non-negative matrix factorization to calculate the muscle

419   synergies needed to predict muscle activations associated with missing EMG data. The MTP tool uses a

420   Hill-type muscle-tendon model with a rigid tendon and assumes that muscles function primarily on the

421   ascending region of their normalized active force-length curves.[118] Users can modify cost terms to

422   specify the region of the normalized force-length curve over which muscles are assumed to operate.

423   Some MTP cost function terms, such as inconsistencies among grouped normalized muscle fiber lengths,

424   calculate the difference between the grouped values relative to their mean. These cost terms are

425   intended to promote similarity in muscle properties within a group under the assumption that similar

426   muscles, such as the three uniarticular vastus muscles, should have similar properties. These muscle

427   groups must be defined within the OpenSim model. Similar cost function terms are also present in NCP.

428   3.1.3 Neural Control Model Personalization

429   The Neural Control Model Personalization tool finds muscle synergies that are as consistent as

430   possible with ID joint moments and, when available, MTP-estimated muscle activations. The NCP tool

431   fits muscle synergies at the level of muscle activations (i.e., after electromechanical delay and activation

432   dynamics) for regions of the body where either all muscle activations are available from the MTP tool

433   (e.g., the right lower extremity) or no muscle activations are available.[119,120] The tool can also be used to

434   find muscle synergies in multiple regions of the body simultaneously - some with and some without

435   previously calculated muscle activations. During the NCP optimization process, grouped muscle

436   properties are maintained and activation-related cost function terms are minimized. Muscle synergies

437   are typically calculated from muscle activations alone using non-negative matrix factorization, and thus

438   the muscle activations reconstructed from the resulting synergies will not closely reproduce ID joint

439   moments when input into a subject's musculoskeletal model. NCP rectifies this issue by optimizing

440   synergy activations and synergy vectors to be consistent with both ID joint moments and available

441   muscle activations simultaneously.

442   The inputs to the NCP tool are a post-JMP OpenSim model as well as data for IK motions, ID loads,

443   muscle-tendon lengths and velocities, muscle moment arms, and, optionally, MTP-calculated muscle

444   activations from one or more motion trials of interest (Figure 7). The OpenSim model must contain

445
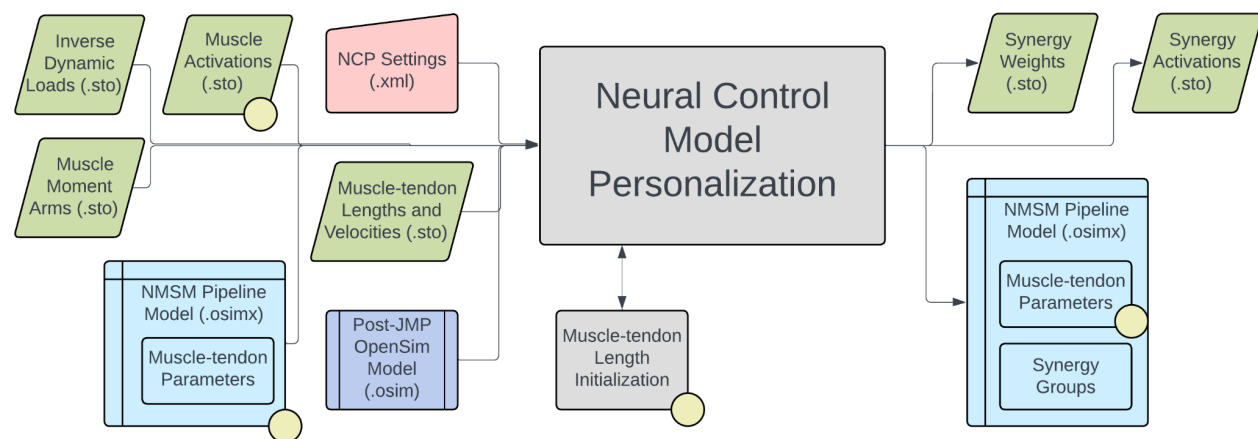
446   **Figure 7:** Flowchart showing the inputs to and outputs from the NCP tool. The diagram key is

447   included in Fig. 5.

448

449   muscle groups that define lists of muscles for which synergy sets are to be fitted (e.g., all right leg

450   muscles). The design variables for the NCP tool are a set of time-varying synergy activations and an

451   associated set of time-invariant synergy vectors. The cost function terms for the NCP tool minimize ID

452   joint moment matching error, MTP muscle activation matching errors, muscle activations,

453   inconsistencies among grouped normalized muscle fiber lengths, and inconsistencies among grouped

454   muscle activations. The NCP tool includes a constraint that the sum of the muscle weights in each

455   synergy vector must equal a constant times the number of muscles described by that synergy. Upon

456   output, the synergy vectors and synergy activations are normalized such that the largest weight in each

23

457   synergy vector is one. The NCP tool produces a set of synergy groups inside a new or pre-existing NMSM

458   Pipeline model file (.osimx) as well as data files (.sto) containing synergy activations and their associated

459   synergy vectors.

460   Several important considerations should be kept in mind when using the NCP tool. Synergy-driven

461   Tracking Optimization (TO), part of the Treatment Optimization toolset, requires that NCP tool results be

462   used as the initial guess. NCP results that distribute errors equally between MTP muscle activation

463   matching and ID joint moment matching will facilitate the process of finding good synergy-driven TO

464   results. In addition, to facilitate obtaining good NCP results, users should perform their own synergy

465   analysis on the muscle activations produced by MTP to determine the optimal number of synergies to

466   use. The number of synergies should be selected to achieve the desired variability accounted for (VAF),

467   which is often set at 90 or 95%.[41,93,121,122] The NCP tool can be run without having MTP tool results as

468   inputs through the use of the activation minimization cost function term. Since running the NCP tool

469   without MTP tool results produces a non-unique solution, the maximum allowable error of the

470   activation minimization cost function term can be set to achieve a unique solution that contains

471   activations of expected magnitude. Shared synergy vectors between synergy groups can also be

472   enforced by the NCP tool. This feature allows for two muscle synergy groups, such as those for right and

473   left leg muscles, to have nearly identical synergy vectors.

474   3.1.4 Ground Contact Model Personalization

475   The Ground Contact Model Personalization tool finds physical properties for elastic foundation foot-

476   ground contact models that closely reproduce experimental ground reaction forces and moments while

477   allowing slight changes in foot kinematics. The elastic foundation is composed of a uniform grid of linear

478   springs with nonlinear damping and friction placed across the bottom of the foot. The tool can

479   personalize ground contact models for each foot separately, where physical properties will differ

480   between the two feet, or both feet together, where physical properties will be the same for the two

24

481   feet. Currently, the tool works with only a two-segment foot model composed of a hindfoot segment

482   (including calcaneus, cuboid, navicular, cuneiform, and metatarsal bones) and a toes segment (including

483   phalange bones). While generic foot-ground contact models can reproduce experimental ground

484   contact forces accurately, they reproduce experimental ground reaction moments less accurately,

485   introducing errors into the lower body joint moments generated by predictive simulations of walking.[79]

486   Personalized foot-ground contact models can overcome this issue by reproducing experimental ground

487   reaction moments as well.

488   The inputs to the GCP tool are a post-JMP lower-body or full-body OpenSim model along with IK

489   motion and associated ground reaction data for a walking trial, where the IK and ground reaction data

490   must possess the same time increments (Figure 8). The ground reaction data must contain three forces,

491
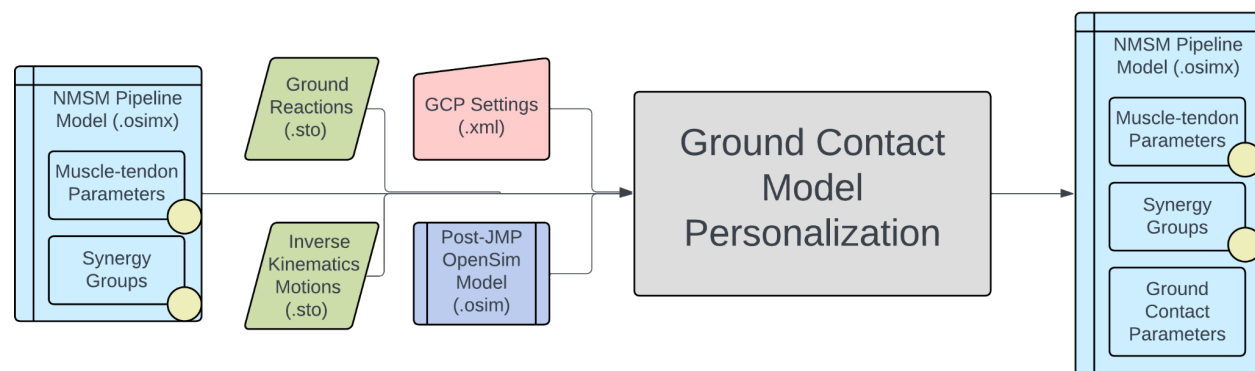
492   **Figure 8:** Flowchart showing the inputs to and outputs from the GCP tool. The diagram key is

493   included in Fig. 5.

494

495   three moments, and a point about which the moments are calculated, which is typically either a time-

496   invariant point fixed in the laboratory or a time-varying center of pressure. The tool automatically strips

497   off both feet from the lower-body or full-body OpenSim model and creates a 6 degrees of freedom

498   (DOF) custom joint connecting each specified hindfoot body to ground. The design variables for the GCP

499   tool are stiffness coefficients unique to each spring with a nonlinear viscous damping coefficient, a

500   dynamic friction coefficient, a viscous friction coefficient, and a spring resting length common to all

501   springs. Additional design variables are B-spline nodal points defining small deviations from

502   experimental foot kinematics with respect to ground. The cost function terms for the GCP tool include

503   minimization of foot marker position errors, foot marker velocity errors, hindfoot and toes segment

504   rotational coordinate errors, hindfoot segment translational coordinate errors, vertical ground reaction

505   force errors, horizontal ground reaction force errors, ground reaction moment errors, and spring

506   coefficient deviations from neighboring spring coefficient values. No constraints are present in this

507   optimization problem. The output of the GCP tool is a new NMSM Pipeline model file (.osimx) containing

508   foot-ground contact model parameter values.

509   Several important considerations should be kept in mind when using the GCP tool. The tool can

510   reproduce all six components of ground reactions with good fidelity. To facilitate reproducing ground

511   reaction moments, we use the time-varying projection of a midfoot superior marker onto the ground as

512   the point about which ground reaction moments are calculated. This automatic recalculation of the

513   ground reaction moments helps keep the moments well-scaled during a GCP run, since the moment arm

514   of the ground reaction force vector never becomes excessively large. The center of pressure is not used

515   for joint moment matching since it becomes inaccurate at the transitions into and out of contact due to

516   division by small vertical ground reaction force values. At this time, the GCP tool requires the use of a

517   two-segment foot model with the distal toes segment connected to the hindfoot segment via an oblique

518   pin joint. Before personalization, the GCP tool automatically extracts two-segment OpenSim foot models

519   from the post-JMP lower-body or full-body OpenSim model and automatically calculates hindfoot

520   kinematics with respect to ground that are consistent with the input lower-body or full-body kinematics.

521   Since the foot-ground contact model is sensitive to foot kinematic changes below the measurement

522   accuracy of a markered motion capture system, the GCP tool allows for small changes to the foot

523   motion trajectory to facilitate ground reaction matching. Each foot model possesses seven coordinates:

524   six ground-to-hindfoot coordinates via a 6 DOF custom joint and one toes coordinate via a pin joint.

26

525   Coordinate deviations are parameterized with B-spline nodes to reduce the number of design variables.

526   The GCP tool automatically estimates the number of B-spline nodes needed based on a specified

527   lowpass filter cutoff frequency. Another important feature of the GCP tool is its ability to use a different

528   time window for calibrating each foot. This feature facilitates the use of the GCP tool with ground

529   reaction data obtained from labs possessing only two in-ground force plates. The GCP tool also allows

530   for symmetric physical properties between contact surfaces on the two feet, and users can modify the

531   number of springs along each dimension of the grid.
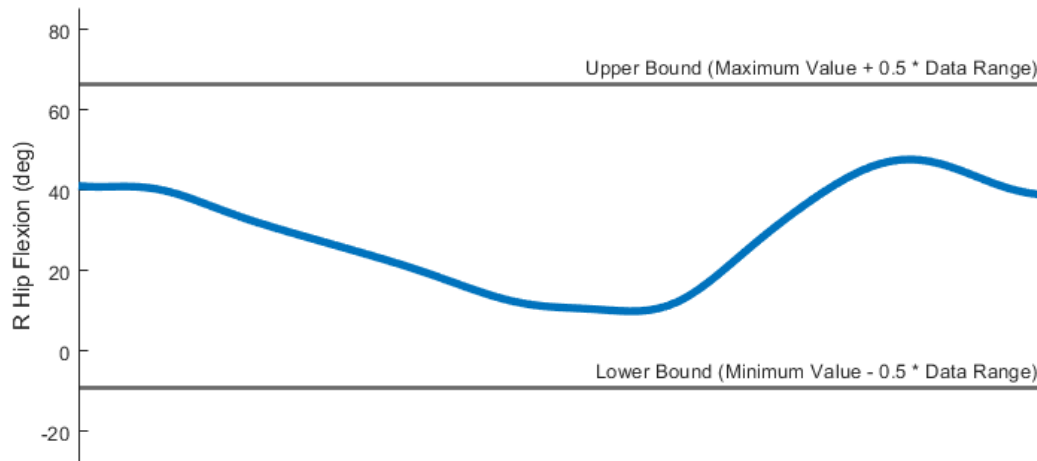
532   ## 3.2 Treatment Optimization

533   The Treatment Optimization toolset generates predictive simulations of a patient's post-treatment

534   movement function by optimizing specified treatment design parameters. The toolset consists of three

535   tools designed using a "theme and variation" approach, where the tools are intended to be used in a

536   specific order, with each tool serving a distinct purpose. Each tool uses the GPOPS-II direct collocation

537   optimal control software for MATLAB[60] and maintains a consistent structure for data inputs, problem

538   design, cost function terms (see Table S1), constraint terms (see Table S2), and outputs, with variations

539   (Figure 9). The Tracking Optimization tool (TO) generates "starting point" predictive simulations of

540
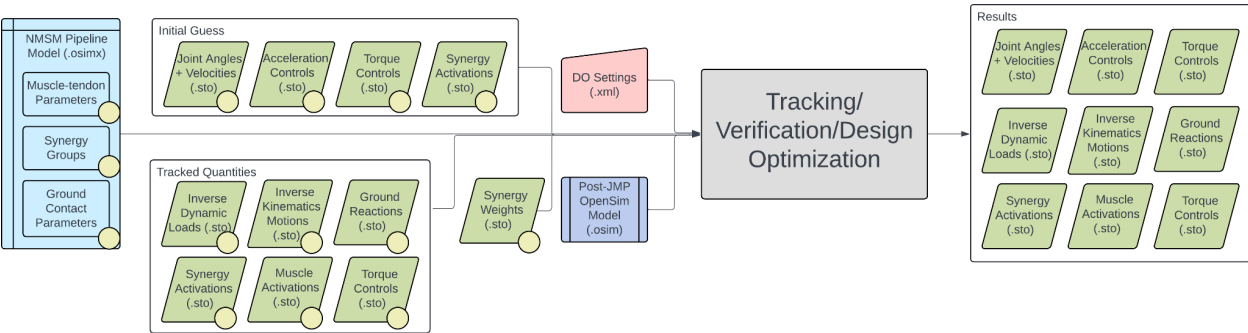
541   **Figure 9:** Flowchart showing the inputs to and outputs from the tools included in the Treatment

542   Optimization toolset. Since these tools follow a theme and variation approach, various data

543   combinations can be included or excluded based on the goals of the user. The diagram key is included in

544   Fig. 5.

27

545

546   patient movement that are dynamically consistent and closely reproduce all relevant experimental

547   movement data available from the patient (e.g., joint motion, joint moment, ground reaction, and EMG

548   data). The Verification Optimization tool (VO) starts from the Tracking Optimization solution and verifies

549   that the controls found produce the correct motion without tracking the motion directly, which ensures

550   that the subsequent treatment design problem is well formulated before simulated treatments are

551   explored. Finally, the Design Optimization tool (DO) starts from the Verification Optimization solution,

552   applies and (if desired) optimizes simulated treatments, and predicts the patient's resulting post-

553   treatment movement along with associated controls and loads. All three tools work with torque

554   controlled, muscle synergy controlled, and combined torque and muscle synergy controlled problem

555   formulations.

556   Several important considerations should be kept in mind when working with the Treatment

557   Optimization toolset. Direct collocation optimal control problems are solved by modifying states and

558   controls simultaneously to minimize an objective function and fulfill constraints. For Treatment

559   Optimization, the states consist of joint positions and velocities for selected OpenSim model coordinates

560   and the controls consist of corresponding joint accelerations (due to the use of an implicit dynamics

561   formulation[59]), torque controls, synergy controls, or both. All Treatment Optimization tools accept both

562   a "tracked quantities" and an "initial guess" directory. The tracked quantities directory contains

563   reference data (e.g., experimental joint positions, joint moments, muscle activation, and ground

564   reactions) to be tracked by specified cost function terms while the initial guess directory contains data

565   specifying the initial guess for the problem's states and controls. Treatment Optimization XML settings

566   files allow for joint position, velocity, and acceleration range scale factors as well as muscle synergy and

567   torque controller range scale factors. These range scale factors describe the search space of the optimal

568   control problem by confining the states and controls to be within a certain range relative to their initial

569   range (see Figure 10). After a completed run, all Treatment Optimization tools output the same files to a

570

571

572   **Figure 10:** Illustration showing how range scale factors are used to set bounds on the states and

573   controls within GPOPS-II. The range scale factor value is used to set the maximum and minimum

574   searchable spaces for the states and controls as offsets beyond the initial range. In this figure, a range

575   scale factor of 0.5 was used.

576

577   user-specified results directory. Specifically, the solution's states and controls, along with IK motions, ID

578   loads, and ground reactions calculated from the solution's states and controls, are output to the

579   specified directory. Saved states and controls can then be passed to the next Treatment Optimization

580   tool as an initial guess to pick up where the previous tool left off.

581   Because Treatment Optimization tools use implicit dynamics,[41,59] several constraint terms must be

582   included for successful use of the toolset. One constraint is that the joint acceleration controls must be

583   the first time derivatives of the joint velocity states, and the joint velocity states must be the first time

584   derivatives of the joint position states. These constraints are handled internally by GPOPS-II. Another

29

585   constraint is that the net joint loads produced by the torque and synergy controls must be consistent

586   with the model's inverse dynamic loads. This constraint must be handled by the user by including kinetic

587   consistency constraint terms for all controlled coordinates included in the problem formulation. In

588   addition, if users want their Treatment Optimization solutions to be dynamically consistent, then the

589   root segment residual load constraint must be included to ensure that the residual loads acting on the

590   model's root segment (i.e., the segment connecting the model to ground) are close to zero. In addition,

591   if the motion of interest is expected to be periodic, such as for walking, running, cycling, or stair-

592   climbing, joint position and velocity and ground reaction force and moment periodicity constraints can

593   be used to ensure that a near-periodic motion is found.

594   3.2.1 Tracking Optimization

595   The Tracking Optimization tool uses a personalized model to produce a dynamically consistent

596   movement simulation that closely reproduces all available experimental motion data, including joint

597   motions, joint moments, ground reaction forces and moments, and muscle activations. To achieve a

598   dynamically consistent motion, the tool spreads out matching errors between the different

599   experimental quantities based on user-specified maximum allowable errors. The tool accepts a post-JMP

600   OpenSim model (.osim file) and personalized NMSM Pipeline model (.osimx file) along with

601   experimental IK motions, ID loads, ground reactions, muscle-tendon lengths and velocities, muscle

602   moment arms, and, if using synergy controls, NCP results for the trial of interest. The following cost

603   function terms are commonly included to achieve a successful Tracking Optimization run: generalized

604   coordinate tracking, generalized speed tracking, inverse dynamic moment tracking, muscle activation

605   tracking, external force tracking, and external moment tracking. Common constraint terms include

606   kinetic consistency, state position periodicity, state velocity periodicity, and root segment residual load

607   bounding.

608   Several important considerations should be kept in mind when using the Tracking Optimization tool.

609   Finding a good result with the Tracking Optimization tool is the biggest challenge in the NMSM Pipeline.

610   The goal is to trade off errors between tracked experimental data sources by modifying the maximum

611   allowable error in each cost function term based on the importance of and confidence in the respective

612   experimental data. Higher quality Model Personalization results and highly consistent tracked

613   experimental quantities (e.g., tracked muscle activations should closely reproduce tracked ID moments)

614   make finding a good Tracking Optimization solution easier.

615   3.2.2 Verification Optimization

616   The Verification Optimization tool is used to perform a "dry run" Design Optimization without

617   including any "design elements", the goal being to ensure a good initial guess and to verify the

618   appropriateness of the optimal control problem formulation. The tool accepts the same inputs as the TO

619   tool, but in general, the results directory of a TO run is used for both the initial guess and tracked

620   quantities. The cost function terms for the VO tool include controller tracking and, for uncontrolled

621   joints, generalized coordinate tracking. Similar to the TO tool, the VO tool includes constraint terms for

622   kinetic consistency, state position periodicity, state velocity periodicity, and root segment residual load

623   bounding. If a VO problem is well formulated, it should converge quickly since the initial guess is already

624   at the optimal solution.

625   Several important considerations should be kept in mind when using the Verification Optimization

626   tool. Users must decide whether each coordinate should be controlled or tracked. If controlled, the

627   coordinate should be assigned the same controller (synergy, torque, or both) as in the TO tool, and the

628   controls should be tracked by the VO tool. Conversely, if the coordinate does not have a controller or

629   has a non-essential controller, then the coordinate should be tracked by the VO tool. An example of a

630   non-essential controller is a torque controller on an upper body joint for a full body gait model with only

631   lower body muscles. The results of a VO run should closely match the outputs of the TO run used to

31

632   define the initial guess and tracked quantities. If the results do not match closely, then a problem

633   formulation issue is likely present, and users should review their TO and VO settings. Examples of

634   potential problem formulation issues are having a generalized coordinate that is neither controlled nor

635   tracked, having a generalized coordinate that is both controlled and tracked, or having a generalized

636   coordinate that is tracked with a different maximum allowable error than was used by TO. Each of these

637   situations can produce a VO solution that differs from the TO initial guess. After an adequate VO

638   solution is found, users can move on to the DO tool by adding a "treatment" to their VO problem

639   formulation.

640   3.2.3 Design Optimization

641   The Design Optimization tool predicts or optimizes how a planned treatment will affect a patient's

642   post-treatment movement function. The tool accepts the same inputs as the other Treatment

643   Optimization tools, but typically VO results are used as the initial guess. Similar to VO, DO allows for

644   controller tracking and generalized coordinate tracking alongside other DO-specific cost function terms.

645   Similar to TO and VO, DO can use kinetic consistency, state position periodicity, state velocity

646   periodicity, and root segment residual load constraint terms as well as other constraints to facilitate the

647   design of a personalized intervention.

648   Several important considerations should be kept in mind when using the Design Optimization tool.

649   Unlike the other Treatment Optimization tools, the DO tool allows for both fixed and free final time

650   problem formulations. For free final time problems, the time vector can be constrained to a user defined

651   range and tracked control quantities are stretched or compressed in time to match the current time

652   vector. A number of built-in cost function terms have been included in the DO tool. These terms include

653   minimizing braking and propulsive impulse errors from target values, metabolic cost per unit of time or

654   distance[123] errors from a relative target value, whole-body angular momentum error from a target

655   value, and joint mechanical energy generation or absorption errors from a target value. Two key

32

656   features of the DO tool are support for model modification functions and user-defined cost function

657   terms. By employing model modification functions alongside GPOPS-II's static parameters feature, users

658   can change the OpenSim musculoskeletal model, modify the neural control model, or adjust parameter

659   values in an assistive device. Possible model modifications include changing bone geometry (e.g.,

660   osteotomy parameters), changing muscle-tendon properties (e.g., strengthening muscles or adjusting

661   optimal muscle fiber lengths), changing neural control properties (e.g., altering synergy vector weights

662   or synergy activation profiles), modifying ground contact model parameters, optimizing muscle

663   attachment locations or muscle wrapping surface parameters, redefining joint parameters, and

664   modifying external device design and/or control parameters. User-defined cost function terms allow

665   users to write a custom MATLAB function, with a specific function signature, that is added as an

666   additional cost function term given the iteration's states, controls, and static parameters.

4. Example Application

4.1 Treatment Design Rationale

669   To demonstrate the capabilities of the NMSM Pipeline, we employed it to investigate a hypothetical

670   treatment to improve walking speed and function for an individual post-stroke. Published studies have

671   hypothesized that time-varying synergy activations originate in the brain while time-invariant synergy

672   vectors reside in the spinal cord.[124,125] If this hypothesis is true, then one might expect a stroke to affect

673   a patient's synergy activations but not synergy vectors.[125] This expectation in turn suggests that an

674   individual post-stroke may have similar synergy vectors between the two legs but lack the ability to

675   recruit one or more of them effectively on the paretic side. Furthermore, published studies have

676   reported that a stroke results in altered neural coordination even on the non-paretic side.[126–128] Taken

677   together, these observations lead to the hypothesis that a stroke may impair recruitment of one or

678   more synergy activations in the paretic leg, resulting in altered recruitment of one or more synergy

33

679   activations in the non-paretic leg, and that restoration of these impaired and altered synergy activations

680   could result in improved self-selected walking speed and metabolic cost.[128–130]

681   To investigate this hypothesis, we used the NMSM Pipeline to design a hypothetical treatment that

682   would modify paretic and non-paretic leg synergy activations for an individual post-stroke with the goal

683   of increasing his self-selected walking speed without increasing his metabolic cost. Previously published

684   experimental walking data collected from an individual post-stroke with a self-selected walking speed of

685   0.5 m/s were used for the investigation.[41] Research has shown that both healthy individuals and

686   individuals post-stroke tend to choose a self-selected walking speed to achieve a desired metabolic cost

687   per unit time.[131] Furthermore, to achieve successful community ambulation (as defined by the walking

688   speed required to cross a typical street before the light changes[132]), individuals should be able to walk at

689   a self-selected speed of 0.8 m/s.[132,133] Thus, the specific goal of the hypothetical treatment was to

690   increase the subject's self-selected walking speed to 0.8 m/s while maintaining the same metabolic cost

691   per unit time estimated for the subject's original self-selected walking speed of 0.5 m/s.

692   4.2 Experimental Data Collection

693   As described in Meyer et al. (2016),[41] the experimental data used for the present study were

694   collected from a high-functioning hemiparetic subject with chronic stroke-related walking dysfunction

695   (sex male, age 79 years, LE Fugl-Meyer Motor Assessment 32/34 pts, right-sided hemiparesis, height 1.7

696   m, mass 80.5 kg). Experimental data collection was approved by the University of Florida Health Science

697   Center Institutional Review Board (IRB-01) and the Malcom Randall VA Medical Center Research and

698   Development Committee, and the subject gave written informed consent prior to participation. Motion

699   capture (Vicon Corp., Oxford, UK), ground reaction (Bertec Corp., Columbus, OH, USA), and

700   electromyography (EMG) data (Motion Lab Systems, Baton Rouge, LA, USA) were collected

701   simultaneously while the subject walked on a split-belt instrumented treadmill with belts tied. The

702   subject walked at his self-selected speed of 0.5 m/s and fastest comfortable speed of 0.8 m/s. To

703   facilitate ground contact model personalization, the subject wore Adidas Samba Classic sneakers, which

704   possess a flat sole with neutral midsole. Motion capture data utilized a full-body marker set with one

705   marker at each toe tip, three markers on each hindfoot, shank, and thigh, three markers on the pelvis,

706   and one marker on each acromion, elbow, and wrist (Reinbolt et al., 2005; Fregly et al., 2007). Ground

707   reaction data from each treadmill force plate included three force and moment components along with

708   the location of the fixed point used for moment calculations. EMG data included a combination of

709   surface and fine-wire electrodes collected from 16 muscles on each leg, including deep muscles

710   adductor longus, iliopsoas, tibialis posterior, extensor digitorum longus, and flexor digitorum longus.

711   Processing of marker motion, ground reaction, and EMG data followed a previously published

712   protocol.[41] Marker motion and ground reaction data were filtered at a variable cut-off frequency of 7/tf

713   Hz, where tf is the period of the gait cycle being analyzed, using a fourth-order zero phase lag

714   Butterworth filter.[134] EMG data were high-pass filtered at 40 Hz,[75] demeaned, rectified, and low-pass

715   filtered at a variable cut-off frequency 3.5/tf Hz using a fourth-order zero phase lag Butterworth filter.

716   Each processed EMG signal was normalized by the maximum value over all walking cycles and then

717   offset so that the minimum value was zero. For both walking speeds, the single most periodic walking

718   cycle (heel strike to heel strike for the paretic right leg) was selected for analysis, and all data for this

719   one cycle were resampled to 101 time points. After resampling, EMG data were padded with 200

720   milliseconds (18 time points) before the start of the cycle to account for electromechanical delay.

721   4.3 Model Personalization Process

722   We utilized all four tools in the Model Personalization toolset to personalize a full-body

723   neuromusculoskeletal model of the subject being studied. The starting point for the model

724   personalization process was a scaled RCNL2023 full-body OpenSim model, where scaling was performed

725   using the OpenSim Model Scaling tool with experimental marker data collected from the subject during

35

726   a static standing trial. All subsequent NMSM Pipeline tool runs were performed on a Dell PC workstation

727   possessing 48 cores.

728   First, the JMP tool was used to personalize lower body joint parameters and lower body scaling by

729   minimizing IK marker distance errors. The selected 0.8 m/s gait cycle marker data were used for all JMP

730   tool tasks. To avoid non-anatomical muscle paths around the hip complex, the left and right hip joint

731   parameters were not personalized. The left and right knee and ankle joints were personalized, but the

732   subtalar joint was not personalized because the joint did not move through a sufficient range of motion

733   to personalize the joint's parameter values accurately. The JMP tool reduced marker distance errors for

734   the thigh, shank, and foot markers by 48.4% for the gait cycle of interest. Additional JMP results are

735   included in Table 1 and in the supplementary material. Convergence was achieved after approximately

736   90 minutes of CPU time.

737

738   **Marker Distance Errors Before and After Joint Model Personalization**

	RMS (mm)		Max (mm)	
	Pre-JMP	Post-JMP	Pre-JMP	Post-JMP
Right Knee	7.5	4.2	18.5	11.8
Right Ankle	6.1	3.3	16.9	9.1
Left Knee	9.5	4.1	26.3	12.8
Left Ankle	6.5	3.2	16.4	10.1

739   **Table 1:** RMS and maximum marker distance errors (mm) for the right and left knee and ankle (including

740   subtalar) joints. Markers included in each joint's JMP marker set included thigh and shank markers for

741   each knee joint and shank and foot markers for each ankle joint. These markers were used to find the

742   pre- and post-JMP RMS and maximum marker distance errors.

743

744   Second, the MTP tool was used to personalize the properties of all lower body muscles by

745   minimizing errors in matching inverse dynamic joint moments and changes in initial muscle-tendon

746   parameter values while also predicting missing EMG signals for deep or "small" muscles (e.g.,

747   piriformis). Before the MTP tool was run, the OpenSim Inverse Kinematics, Inverse Dynamics, and

748   Muscle Analysis tools were run from the OpenSim GUI using the selected 0.8 m/s walking cycle data.

749   Using the outputs of these GUI tools, an NMSM Pipeline utility script processed EMG data, calculated

750   muscle-tendon velocity from muscle-tendon length data, and automatically organized the trial data into

751   the directory structure required by the MTP tool. Muscle groups were added to the post-JMP OpenSim

752   model to group muscles based on normalized fiber length similarity and activation similarity. Muscle-

753   tendon Length Initialization was used to find initial values for optimal muscle fiber length and tendon

754   slack length. At that point, muscle-tendon model and activation dynamics parameter values were

755   personalized. This process was repeated for each leg separately via separate runs of the MTP tool. After

756   the MTP tool was run for both legs, the left leg was found to match lower body joint moments with an

757   average root mean square (RMS) error of 3.5 Nm and the right leg with an average RMS error of 2.1 Nm.

758   Joint-specific moment matching results are included in Table 2 with additional plots available in the

759   supplementary material. A custom script was used to combine the left and right leg results for use by

760   the NCP tool. Convergence was achieved after approximately 30 minutes of CPU time.

761

762   **Lower Body Joint Moment Matching Errors following Muscle-tendon Model Personalization**

Joint Coordinate	Hip Flexion	Hip Adduction	Hip Rotation	Knee Angle	Ankle Angle	Subtalar Angle

37

Right (Nm)	2.9	2.7	3.1	1.7	1.0	1.5
Left (Nm)	5.8	4.3	4.8	2.2	2.4	1.5

763 **Table 2:** RMS errors between net joint moments calculated by the OpenSim ID tool and those calculated

764 by the NMSM Pipeline MTP tool following muscle-tendon model personalization.

765

766   Third, the NCP tool was used to calculate lower body muscle synergies (i.e., synergy vectors and

767 activations) by minimizing errors in matching inverse dynamic joint moments and muscle activations

768 produced by the MTP tool. Given our treatment design rationale above, we assumed that the subject's

769 synergy vectors were the same while his synergy activations were different for the two legs. As a result,

770 the NCP tool was used with the bilateral synergy vector symmetry option enabled. Synergy sets were

771 defined as muscle groups denoting the right and left legs. A previous synergy analysis performed on the

772 subject's processed EMG data indicated that six synergies were sufficient to account for the signal

773 variability even with the added synergy vector symmetry constraint. Muscle Tendon Length Initialization

774 was not performed as part of this NCP tool run because all muscles had MTP-derived muscle activations

775 and thus the activation minimization term was not used. The muscle synergies found by the NCP tool

776 reproduced all lower body joint moments with an average RMSE of 2.2 Nm and all MTP-derived muscle

777 activations with an average RMSE of 0.034. Additional NCP results are included in Table 3 and in the

778 supplementary material. Convergence was achieved after approximately 3 hours of CPU time.

779

780   **Lower Body Joint Moment Matching Errors following Neural Control Model Personalization**

Joint Coordinate	Hip Flexion	Hip Adduction	Hip Rotation	Knee Angle	Ankle Angle	Subtalar Angle
Right (Nm)	1.2	2.2	2.9	2.7	1.0	1.5
Left (Nm)	1.6	3.0	3.4	2.8	2.4	1.7

781   **Table 3:** RMS errors between net joint moments calculated by the OpenSim ID tool and those calculated

782   by the NMSM Pipeline NCP tool following neural control model personalization using muscle synergies.

783

784   Fourth, the GCP tool was used to personalize foot-ground contact model parameter values by

785   minimizing errors in matching ground reaction forces, ground reaction moments, and foot kinematics. A

786   contact element grid size of 5 by 11 was selected to match previous successful investigations.[79] The cost

787   functions for the three tasks performed by the tool were dominated by terms that emphasized matching

788   the vertical GRF, vertical and horizontal GRF, and vertical and horizontal GRF as well as ground reaction

789   moments, respectively, with each task starting from the solution of the previous task to track additional

790   quantities dependent on the previous quantities. To facilitate smooth ground reaction forces during

791   Treatment Optimization, we used the viscous friction coefficient as a design variable and turned off

792   dynamic friction. The viscous friction model penalizes excessive foot velocity with respect to the ground

793   during ground contact, which could lead to excessive horizontal GRFs in predictive simulations. The GCP

794   tool produced a personalized non-uniform distribution of spring stiffness coefficients and matched

795   ground reaction forces, ground reaction moments, foot positions, and foot orientations with RMSEs of

796   4.6 N, 2.1 Nm, 6.4 mm, and 1.7 degrees, respectively.[135,136] Additional GCP results are included in Table 4

797   and in the supplementary material. Convergence was achieved after approximately 4 hours of CPU time.

798

799   **Ground Reaction Force/Moment and Foot Position/Orientation Errors following Ground Contact**

800   **Model Personalization**

Ground Reaction Forces and Moments	Anterior Force (N)	Vertical Force (N)	Lateral Force (N)	X Moment (Nm)	Y Moment (Nm)	Z Moment (Nm)	
Right	3.5	10.2	0.9	4.6	0.9	2.0	
Left	4.1	7.4	1.3	1.8	1.1	2.1	

39

Foot Positions and Orientations	X Translation (mm)	Y Translation (mm)	Z Translation (mm)	X Rotation (deg)	Y Rotation (deg)	Z Rotation (deg)	Toe Angle (deg)
Right	5.6	10.1	6.5	0.5	1.1	3.7	1.3
Left	4.9	6.6	4.8	2.1	1.7	2.5	1.2

801 **Table 4:** RMS errors between ground reaction forces and moments measured experimentally, and foot

802 positions and orientations measured experimentally and those calculated by the NMSM Pipeline GCP

803 tool following ground contact model personalization.

804

805 4.4 Treatment Optimization Process

806 After personalizing the subject's neuromusculoskeletal model using all four Model Personalization

807 tools, we ran all three Treatment Optimization tools to predict how underutilized paretic and non-

808 paretic leg synergy activations should be upregulated to achieve a 0.8 m/s self-selected walking speed

809 without increasing metabolic cost per unit time above the subject's 0.5 m/s level.

810 First, the TO tool was used to generate a dynamically consistent full body walking motion at 0.8 m/s

811 that closely reproduced the subject's joint motion, joint moment, ground reaction, and muscle

812 activation data simultaneously using muscle synergy controls for the lower body and joint torque

813 controls for the back and upper body. Since synergy-driven TO requires an initial guess for synergy

814 vectors and activations, the TO tool XML settings file was configured such that the initial guess directly

815 was defined to be the NCP results directory while the tracked quantities directory was defined to be the

816 preprocessed data directory created after running the JMP tool. Other information, including an NMSM

817 Pipeline model file (.osimx), the post-JMP RCNL2023 OpenSim model, and the specified output

818 directory, were also included in the TO tool XML settings file. All lower body joints were controlled by

819 synergy controllers except for the toes coordinate, which was left uncontrolled, and all other joints were

820 controlled by torque controllers. Cost function terms tracked joint positions and velocities found by a

40

821   post-JMP IK analysis, joint moments found by a post-JMP ID analysis (excluding pelvis residual loads),

822   muscle activations found by MTP, and external loads consisting of processed experimental ground

823   reaction data. Constraint terms included bounded kinetic consistency errors (0.01 Nm) for all controlled

824   joints, root segment residual loads for the pelvis (1 N for forces and 0.1 Nm for moments), and joint

825   position periodicity errors (0.05 rad for joints below the pelvis and 0.1 rad for joints above it). The

826   solution produced by the TO tool matched tracked joint positions with an average RMSE of 2.1 degrees,

827   joint moments with an average RMSE of 5.1 Nm, ground reaction forces with an average RMSE of 25.3

828   N, ground reaction moments with an average RMSE of 4.0 Nm, and muscle activations with an average

829   RMSE of 0.038. Additional TO results are included in Table 5 and in the supplementary material.

830   Convergence was achieved after 305 IPOPT iterations, which required approximately 770 minutes of

831   CPU time.

832   **Lower Body Tracking Optimization Errors Relative to Experimental Data**

	Joint Angles (deg)	Joint Moments (Nm)	Ground Reaction Forces (N)	Ground Reaction Moments (Nm)	Muscle Activations
Right	2.7	4.0	22.8	4.3	0.037
Left	3.1	4.8	27.9	3.7	0.039

833   **Table 5:** RMS errors between joint angles, joint moments, ground reaction forces, ground reaction

834   moments, and muscle activations for the right and left legs obtained from experimental data and

835   corresponding quantities predicted by the NMSM Pipeline TO tool.

836

837   Second, the VO tool was used to verify that tracking the muscle synergy controls and upper body

838   joint kinematics found by the TO tool reproduced the joint motions, joint moments, and ground

839   reactions predicted by the TO tool without tracking those quantities explicitly. For the VO run, the

840   results of the previous TO run were used for both the initial guess and tracked quantities data. Cost

41

841   function terms tracked TO-found synergy controls and TO-found torque-controlled joint positions.

842   Constraint terms included bounded kinetic consistency errors (0.01 Nm) for all controlled joints, root

843   segment residual loads for the pelvis (1 N for forces and 0.1 Nm for moments), and joint position

844   periodicity errors (0.05 rad for joints below the pelvis and 0.1 rad for joints above it). The solution

845   produced by the VO tool matched tracked joint positions with an average RMSE of 0.1 deg, joint

846   moments with an average RMSE of 0.1 Nm, ground reaction forces with an average RMSE of 0.7 N,

847   ground reaction moments with an average RMSE of 0.1 Nm, and muscle activations with an average

848   RMSE of 0.01. Additional MTP results are included in Table 6 and in the supplementary material.

849   Convergence was achieved after 101 IPOPT iterations, which required approximately 170 minutes of

850   CPU time. Since the VO results closely matched the TO results, we were confident that the controller

851   and joint position tracking cost function terms and associated constraint terms selected for the

852   verification optimization could be used as the basis for the design optimization.

853   **Lower Body Verification Optimization Errors Relative to Tracking Optimization Results**

	Joint Angles (deg)	Joint Moments (Nm)	Ground Reaction Forces (N)	Ground Reaction Moments (Nm)	Muscle Activations
Right	0.09	0.06	0.44	0.06	0.01
Left	0.08	0.09	0.97	0.09	0.01

854   **Table 6:** RMS errors between joint angles, joint moments, ground reaction forces, ground reaction

855   moments, and muscle activations for the right and left legs obtained from the NMSM Pipeline TO tool

856   and corresponding quantities predicted by the NMSM Pipeline VO tool.

857

858   Finally, the DO tool was used to explore whether upregulating underutilized synergy activations in

859   the paretic leg and downregulating overutilized synergy activations in the non-paretic legs could

860   produce a faster self-selected walking speed of 0.8 m/s while maintaining the same metabolic cost per

42

861   unit time calculated for the subject's original self-selected walking speed of 0.5 m/s. The hypothesis in

862   this problem formulation is that large differences in synergy activation amplitudes between the two legs

863   are indicative of impaired paretic leg synergy activations that are smaller than desired and

864   compensatory non-paretic leg synergy activations that are larger than desired. When we evaluated the

865   synergy activations found by VO for the two legs, we identified four pairs that varied significantly in

866   amplitude between the left and right sides. Based on this observation, we formulated a DO problem that

867   sought to bring these four synergy activations with disparate amplitudes in the two legs closer to each

868   other. Each pair of asymmetric synergy activations contained a "weak" and "strong" side. First, scaled-

869   up "weak" synergy activations were tracked for each pair to increase their amplitudes. Second, a custom

870   user-defined cost function was written to reward synergy amplitude similarities between the "weak"

871   and "strong" synergy activations. A user-defined static parameter was added for each of the four

872   synergy pairs representing the amplitude scale factor to be applied to the "strong" synergy activation

873   using a user-defined model modification function. These two terms increased weak synergy activations

874   and encouraged over-active synergy activations to reduce to more symmetric magnitudes while not

875   overconstraining the control space. In addition, a cost function term was added to find a solution with a

876   metabolic cost per unit time that matched the value calculated for the subject's original 0.5 m/s self-

877   selected walking speed. This value was 90% of the original value calculated for the subject's 0.8 m/s self-

878   selected walking speed, making a 10% reduction to the target value. Cost function terms also tracked

879   VO-found synergy controls for the two symmetric control pairs and VO-found torque controls.

880   Constraint terms included bounded kinetic consistency errors (0.01 Nm) for all controlled joints, root

881   segment residual loads for the pelvis (1 N for forces and 0.1 Nm for moments), and joint position

882   periodicity errors (0.05 rad for joints below the pelvis and 0.1 rad for joints above it). The VO results

883   were used in both the initial guess and tracked quantities data directories, and the final time was fixed

884   at the value determined experimentally for the selected 0.8 m/s walking trial.

885   The DO predictive simulation produced modified kinematics, synergy activations, and ground

886   reactions that reduced the subject's metabolic cost per unit time by 9.9% for the selected gait cycle and

887   achieved closely matching maximum amplitudes for the four modified synergy activations. Final results

888   are plotted in Figure 11. Convergence was achieved after 489 IPOPT iterations, which required

889   approximately 730 minutes of CPU time. These DO results suggest that upregulating weak paretic leg

890   synergy activations while downregulating paired non-paretic leg synergy activations could potentially

891   allow the modeled subject to increase his self-selected walking speed by 60% without increasing his

892   metabolic cost per unit time.

893

44
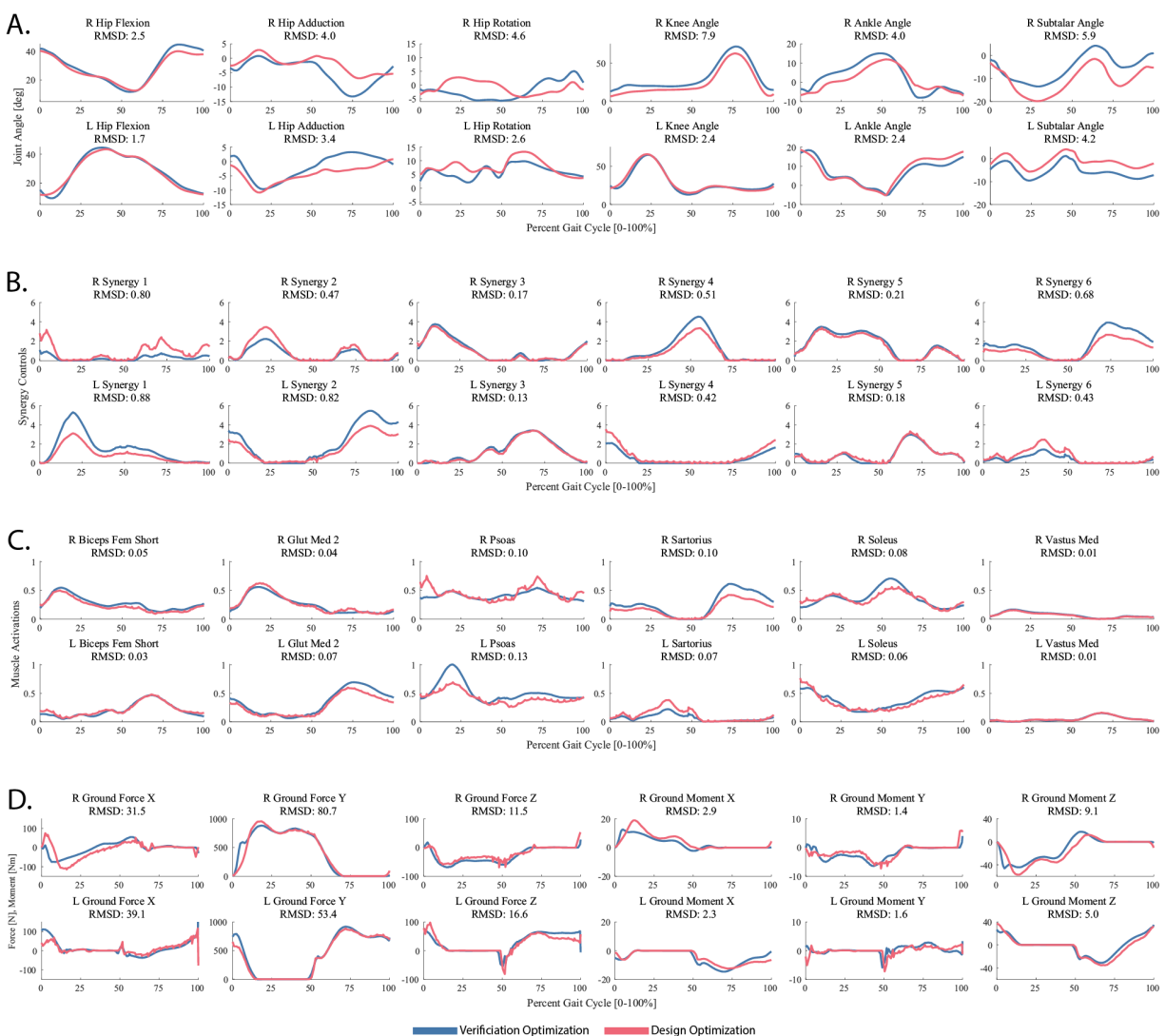
894   **Figure 11:** Plots showing the final results of the DO tool. Subfigures A) kinematics, B) synergy activations,

895   C) muscle activations, and D) ground reaction forces and moments after VO (blue) and DO (red),

896   respectively.

Discussion

898   The primary objective of this work was to develop a novel set of easy-to-use computational tools

899   that facilitate the creation of personalized neuromusculoskeletal models and the subsequent design of

900   personalized clinical treatments by researchers and clinicians with little to no programming experience.

901   These tools dramatically reduce the barrier to entry for researchers and clinicians working together who

902   would like to explore using personalized computational neuromusculoskeletal models to design

903   personalized treatment approaches. As shown in the example application, the NMSM Pipeline has the

904   potential to change the way treatments are investigated and applied throughout the

905   neuromusculoskeletal injury space.

906   Going forward, two key questions need to be addressed if the NMSM Pipeline is to be used to design

907   actual clinical treatments for actual patients. The first question is, how should the patient's personalized

908   model and neural control strategy be changed in response to the simulated treatment? The second

909   question is, how can one validate a patient's predicted post-treatment movement function? The

910   answers to these two questions will depend on the specific clinical application and which aspects of the

911   patient's neuromusculoskeletal system need to be modeled and personalized to investigate that

912   application. The answers will also involve developing an understanding of how the planned intervention

913   will affect a patient's model parameter values and neural control strategy. Collection of post-

914   intervention movement data will be required so that the entire Model Personalization and Treatment

915   Optimization process can be evaluated, refined, and ultimately validated for one clinical application at a

916   time.

917   To conceptualize how these two important questions could be addressed, one can consider two

918   NSM Pipeline clinical applications being explored by the authors - one involving knee osteoarthritis

919   rehabilitation design, and one involving pelvic cancer surgical planning. Past computational research

920   involving a subject with bilateral medial compartment knee osteoarthritis investigated whether

921   personalized gait modifications could be designed to reduce the subject's peak adduction moment in

922   both knees to an extent comparable to invasive high tibial osteotomy surgery [write reference in

923   (author, year) form]. For this treatment optimization problem, no muscles or neural control needed to

924   be modeled, which simplified the treatment design process. The computational treatment design

925   process involved: a) creating a personalized full-body dynamic skeletal model of the subject using pre-

926   rehabilitation gait data, b) selecting a post-treatment control approach to be used when predicting post-

927   treatment walking function (in this case, minimize changes in lower body joint moments relative to pre-

928   rehabilitation gait data), c) performing a treatment optimization process with the personalized model

929   and selected control approach to identify gait modifications that would offload the medial compartment

930   of both knees, d) training the subject to perform and consolidate the modified walking motion, and

931   finally e) re-testing the subject in a gait lab to evaluate how well the predicted gait modifications could

932   reduce both peak adduction moment peaks. After informal training, the subject was able to perform the

933   predicted gait modifications and achieve bilateral reductions in the peak knee adduction moment that

934   were comparable to the treatment optimization predictions. A similar computational treatment design

935   process is currently being repeated using the NMSM Pipeline except with greater flexibility in the range

936   of potential gait modifications that can be predicted.

937   Ongoing computational research involving subjects with pelvic cancer is investigating whether

938   surgical decisions can be planned to achieve a post-surgery gait motion and self-selected walking speed

939   that is as close to normal as possible for each patient[68,137]. For this treatment optimization problem,

940   both muscles and neural control need to be modeled, which complicates the treatment design process.

941 The computational treatment design process being explored involves: a) creating a personalized full-

942 body dynamic neuromusculoskeletal model of the patient using pre-surgery gait, EMG, and imaging data

943 (to personalize pelvis bony geometry), b) selecting a post-surgery control approach to be used when

944 predicting post-surgery walking function (in this case, minimize changes in muscle synergy quantities

945 relative to pre-surgery EMG data)[137], c) performing a treatment optimization process with the

946 personalized model and selected control approach to identify surgical decisions that achieve clear

947 margins while also maximizing recovery of normal walking function[68], d) having the orthopedic

948 oncologist perform the patient's surgery using the optimized surgical plan, and finally e) re-testing the

949 patient in a gait lab following plateau in recovery to evaluate how well the predicted surgical plan

950 allowed the patient to achieve the predicted post-surgery gait motion and speed. Since trial and error

951 treatment is not possible with orthopedic surgeries, extensive testing, evaluation, and refinement of this

952 treatment optimization process must be performed before actual surgical plans can be designed for

953 actual pelvic cancer patients. To this end, the authors are collecting extensive pre- and post-surgery gait,

954 EMG, and imaging data sets from this patient population, along with the implemented surgical

955 decisions. Only after the NMSM Pipeline can predict post-surgery walking function reliably for multiple

956 patients when post-surgery walking function and the implemented surgical decisions are known can the

957 NMSM Pipeline be considered for actual use in this clinical application. A similar process would need to

958 be followed for any other clinical problem to which the NMSM Pipeline would be applied.

959 Although the decision to use MATLAB for the NMSM Pipeline facilitates development and ease of

960 access for users, the decision does create several limitations. C++ and other similar compiled

961 programming languages generally run significantly faster than interpreted programming languages like

962 MATLAB. However, they also introduce challenges since few engineering researchers are strong C++

963 programmers, and system-specific build procedures can often be complicated.[138,139] Due to these

964 drawbacks, most biomechanics software written in compiled languages can be modified only by

965   reporting a bug or requesting a feature and waiting for experienced software developers to release a

966   new version of the software. The NMSM Pipeline actively encourages modifications, bug fixes, and

967   improvements through open-source easy-to-modify MATLAB toolsets. Other interpreted programming

968   languages like Python can struggle with package management, virtual environments, and/or

969   dependency version mismatches that increase barriers to use. MATLAB's native debugging tools,

970   English-readable error messages, and robust, stable core functions allow for development with

971   confidence, making the NMSM Pipeline robust to issues common to other interpreted languages.

972   Our hope is that the NMSM Pipeline's open-source, easy-to-use framework will encourage

973   investigations by the research community into "best practices" for each of the included tools. With the

974   availability of seven new tools, each with many optional features, the research community is

975   encouraged to explore novel approaches to achieving the best results from each tool. Investigations into

976   changes in task order, data processing/organization, cost function error centers and maximum allowable

977   errors, among others, will inform the entire research community on the best ways to leverage these

978   unique tools for successful future research and clinical outcomes.

979   We are already planning future enhancements to improve the versatility and applicability of the

980   NMSM Pipeline to a broader range of clinical and research problems. Potential enhancements would

981   allow greater flexibility and customization during use of the Model Personalization toolset. Support for

982   compliant tendon muscle models and muscle models that differentiate between fast and slow twitch

983   fibers in the MTP tool could facilitate muscle-tendon model personalization and simulation for "fast"

984   activities like running or jumping.[61,140] Support for time-delayed sensory feedback models in the NCP

985   tool could enable investigation of how spasticity, hyperreflexia, and hypertonia interact with

986   incoordination and weakness to produce functional impairment in individuals with an upper motor

987   neuron pathology. Support for multi-segment foot models in the GCP tool could facilitate higher fidelity

988   simulations of foot biomechanics and better reproduction of ground reaction moments. Other potential

989   enhancements could facilitate novel use of the Treatment Optimization toolset. User-defined controls,

990   time-delayed sensory feedback controls, and individual muscle controls could facilitate computational

991   design of personalized functional electrical stimulation protocols[67] and prediction of how

992   downregulating overactive reflexes could improve an individual's movement function. Support for user-

993   defined loads as a function of model states and controls and making it easy to add new states and

994   controls to a DO problem could facilitate computational design of personalized passive and/or active

995   exoskeletons, which would be added to a subject's personalized model after TO and VO had been

996   performed. An enhancement supporting multi-phase optimal control problems, where each phase

997   simulates a different movement cycle with control information shared across phases, could facilitate

998   simulating neural feedback mechanisms, neural adaptation, and cycle-to-cycle motion and control

999   variability. Enhancements supporting the use of closed-chain kinematic models would facilitate

1000   simulation of shoulder models with improved kinematic fidelity for surgical, exoskeleton, and exercise

1001   equipment applications. Support for connecting NMSM Pipeline controls to any type of OpenSim

1002   actuator could allow exploration of alternative optimal control problem formulations that significantly

1003   improve IPOPT convergence rate, especially for TO. Finally, for both toolsets, development of easy-to-

1004   use MATLAB utility functions that automatically process experimental movement data and put it into a

1005   format that can be used directly by NMSM Pipeline tools, without requiring any manual data

1006   manipulation, would make the toolsets accessible to a wider user base.

1007   With all of these potential future enhancements, several limitations and challenges in future NMSM

1008   Pipeline development exist. First, the quality of the personalization results found by the Model

1009   Personalization tools is limited by the quality and quantity of collected experimental data. At this time, it

1010   can be challenging to collect all of the experimental data needed to exercise all seven NMSM Pipeline

1011   tools with a synergy-driven neuromusculoskeletal model. Leveraging markerless motion capture or

1012   inertial measurement units could potentially increase the ability of researchers to collect the movement

49

1013   data required to perform a high-quality pipeline run-through. For Model Personalization, because

1014   gradient-based optimization techniques are used, solutions may become entrapped in a local minimum,

1015   though the final solution will still be better than the initial guess. The use of muscle activations rather

1016   than excitations for the NCP tool and the Treatment Optimization toolset is another limitation, though

1017   back calculation of muscle excitations from muscle activations could potentially be performed given

1018   estimates of activation dynamics parameter values. Using the OpenSim framework through the

1019   OpenSim MATLAB API prevents the NMSM Pipeline from using automatic differentiation to speed up

1020   optimizations performed during the Model Personalization or Treatment Optimization process.

1021   Computations leveraging the OpenSim MATLAB API are inefficient, and speed limitations inherent to this

1022   framework cannot be overcome.

1023   Several research teams have released novel software tools for the musculoskeletal modeling

1024   research community[51–58], and these tools could be used synergistically with the NMSM Pipeline. As

1025   shown in Table 7, though none of these tools possess the broad range of model personalization and

1026   treatment optimization capabilities available in the NMSM Pipeline, all of these tools facilitate some

1027   aspect of creating scaled musculoskeletal models that incorporate personalized bone geometry and

1028   muscle attachment locations. Consequently, these tools can provide the scaled musculoskeletal model

1029   required as a starting point for the NMSM Pipeline Model Personalization process. For example,

1030   NMSBuilder, MAP Client, Torsion Tool, Bone Deformation Tool, or OpenSim Creator could be used to

1031   create personalized bone models from imaging data or physical measurements[52–55,57,141,142]. SimCP,

1032   NMSBuilder, MAP Client, or OpenSim Creator could then be used to personalize muscle attachment

1033   locations[51–53,57]. Next, SimCP, NMSBuilder, MAP Client, AddBiomechanics, or Scale Tool could be used to

1034   create a scaled OpenSim musculoskeletal model possessing the personalized bone geometry and muscle

1035   attachments[51–53,56]. In addition, AddBiomechanics could potentially be used to perform limited initial

1036   personalization of joint functional axes[56], while SimCP could be used to perform initial personalization of

1037   optimal muscle fiber lengths, tendon slack lengths, and synergy control properties[51].

1038

1039 **Comparison of Functionality Available in the NMSM Pipeline and Other Musculoskeletal Modeling Software Tools**

Software Tool	Personalize Bone Geometry	Personalize Muscle Attachments	Scale Generic Models	JMP	MTP	NCP	GCP	TO	VO	DO
NMSM Pipeline	No (1)	No	No	Yes	Yes	Yes	Yes	Yes	Yes	Yes
SimCP	No (1)	Yes	Yes	No	Yes	Yes	No	No	No	No
NMS Builder	Yes	Yes	Yes	No	No	No	No	No	No	No
MAP Client	Yes	Yes	Yes	No	No	No	No	No	No	No
Torsion Tool	Yes	No	No	No	No	No	No	No	No	No
Bone Deformation Tool	Yes	No	No	No	No	No	No	No	No	No
AddBiomechanics	No	No	Yes	Yes (2)	No	No	No	No	No	No
OpenSim Creator	Yes	Yes	No	No	No	No	No	No	No	No
Automatic Scale Tool	No	No	Yes	No	No	No	No	No	No	No

1040 (1) Personalized bone models produced using image processing and surface fitting software (e.g., Mimics, Materialize, Leuven, Belgium;
1041   Geomagic Wrap, Oqton, Ghent, Belgium) can be added.
1042 (2) Some, but not all, of the features of JMP

1043

1044   As shown in Table 7 above, a current limitation of the NMSM Pipeline is the lack of functionality to

1045   personalize a patient's bone morphology to clinical imaging data. The NMSM Pipeline was specifically

1046   designed to avoid the use of imaging data and require only experimental data typically collected in a

1047   human movement lab. However, personalized bone geometry generated using existing methods and

1048   software tools[143,53,137] can easily be incorporated into scaled generic OpenSim models with personalized

1049   joint functional axes[137] to produce more accurate muscle tendon lengths, moment arms, and joint and

1050   bone loading scenarios.

1051   Treatment Optimization also does not currently include a muscle fatigue model. To date, few muscle

1052   fatigue models for neuromusculoskeletal modeling applications have been published in the

1053   literature[144,145]. Thus, selecting an appropriate existing muscle fatigue model would be challenging.

1054   Availability of a muscle fatigue model could improve the utility of predictive simulations for athletic,

1055   other high-intensity, or long duration movements, making this research area an important one for

1056   future investigation.

1057   The NMSM Pipeline's Treatment Optimization toolset has key differences in design and

1058   implementation from the existing OpenSim Moco tool. While Moco is generally the faster software due

1059   to its C++-based implementation, Treatment Optimization leverages the flexibility of MATLAB and

1060   GPOPS-II to facilitate novel features. Current unique features include user-defined functions and the use

1061   of .osimx personalized model components, while future unique features could include support for multi-

1062   phase optimal control problems, as discussed above. Treatment Optimization was designed to be

1063   accessible to both novice and advanced users through intuitive XML settings files, whereas Moco users

1064   typically set up problems through MATLAB or Python scripts. Even so, Moco's implementation facilitates

1065   potential use of C++ automatic differentiation libraries to improve computational speed for gradient

1066   calculations, resulting in more efficient optimizations. Lastly, Moco is free while both MATLAB and

1067   GPOPS-II are commercial products with significant academic discounts. By incorporating NMSM Pipeline

53

1068   model components into native OpenSim in the future, we plan to give users the option of using their

1069   NMSM Pipeline personalized models in either our Treatment Optimization toolset or OpenSim Moco,

1070   allowing the research community to explore the tradeoffs between these two approaches to developing

1071   predictive simulations.

1072   In conclusion, the NMSM Pipeline represents a significant step forward in the ability to personalize

1073   neuromusculoskeletal computer models to patient movement data and then optimize parameters of

1074   potential treatments using the personalized models. The software assembles over two decades of

1075   biomechanics research into a well-designed and accessible framework that makes previously "high end"

1076   modeling, simulation, and optimization techniques accessible to the entire research community. Our

1077   hope is that by empowering researchers and clinicians working together to explore clinically relevant

1078   questions and to design novel personalized interventions, the NMSM Pipeline will bring

1079   neuromusculoskeletal computer modeling not only to the doorstep of clinical utility but also across it.

1080   # Declarations

1081   ## Ethics Approval and Consent to Participate

1082   The de-identified experimental walking data used in this study were collected and disseminated as part

1083   of a previously published study.[41]

1084   ## Consent for Publication

1085   Not applicable.

1086   ## Availability of Data and Materials

1087   The NMSM Pipeline software, along with all data, models, and settings files described in this article, are

1088   available from the "Neuromusculoskeletal Modeling (NMSM) Pipeline" project on SimTK.org

1089   (https://simtk.org/projects/nmsm). Users are welcome to share feedback and request new functionality

1090   through this project's forum. Documentation including implementation details, examples, and tutorials

1091   is available at https://nmsm.rice.edu.

1092   Further details on the NMSM Pipeline software are provided below:

1093   Project name: Neuromusculoskeletal Modeling Pipeline

1094   Project home page: https://nmsm.rice.edu

1095   Archived version:

1096   Operating systems: Windows, MacOS

1097   Programming language: MATLAB

1098   Other requirements: Version 2023a or higher

1099   License: Apache 2.0

1100   The software has no restrictions for use by non-academics.

1101   ## Competing Interests

1102   The authors declare no competing interests.

1103   ## Funding

1107   ## Authors' Information

1108   Claire V. Hammond - cvhammond@rice.edu

1109   Spencer T. Williams - stwilliams@rice.edu

1110   Marleny M. Vega - marlenyarones101@gmail.com

1111   Di Ao - aodi@nwpu.edu.cn

1112   Geng Li - geng.li@rice.edu

1113   Robert M. Salati - rsalati@rice.edu

1114   Kayla M. Pariser - kayla.pariser@rice.edu

1115   Mohammad S. Shourijeh - mohammad.sharifshourijeh@uth.tmc.edu

1116   Ayman W. Habib - ahabib@stanford.edu

1117   Carolynn Patten - cpatten@ucdavis.edu

1118   Benjamin J. Fregly - fregly@rice.edu

1119   Acknowledgments

1124   # References

1125   (1)   Ma, V. Y.; Chan, L.; Carruthers, K. J. The Incidence, Prevalence, Costs and Impact on Disability of
1126   Common Conditions Requiring Rehabilitation in the US: Stroke, Spinal Cord Injury, Traumatic
1127   Brain Injury, Multiple Sclerosis, Osteoarthritis, Rheumatoid Arthritis, Limb Loss, and Back Pain.
1128   *Arch. Phys. Med. Rehabil.* **2014**, *95* (5), 986-995.e1. https://doi.org/10.1016/j.apmr.2013.10.032.
1129   (2)   Ovbiagele, B.; Goldstein, L. B.; Higashida, R. T.; Howard, V. J.; Johnston, S. C.; Khavjou, O. A.;
1130   Lackland, D. T.; Lichtman, J. H.; Mohl, S.; Sacco, R. L.; Saver, J. L.; Trogdon, J. G.; American Heart
1131   Association Advocacy Coordinating Committee and Stroke Council. Forecasting the Future of
1132   Stroke in the United States: A Policy Statement from the American Heart Association and
1133   American Stroke Association. *Stroke* **2013**, *44* (8), 2361–2375.
1134   https://doi.org/10.1161/STR.0b013e31829734f2.
1135   (3)   Theis, K. A.; Roblin, D. W.; Helmick, C. G.; Luo, R. Prevalence and Causes of Work Disability among
1136   Working-Age U.S. Adults, 2011-2013, NHIS. *Disabil. Health J.* **2018**, *11* (1), 108–115.
1137   https://doi.org/10.1016/j.dhjo.2017.04.010.
1138   (4)   Praemer, A.; Furner, S.; Rice, D. P. *Musculoskeletal Conditions in the United States*; American
1139   Academy of Orthopaedic Surgeons: Rosemont, IL, 1999.
1140   (5)   Clark, M. S.; Smith, D. S. Factors Contributing to Patient Satisfaction with Rehabilitation Following
1141   Stroke. *Int. J. Rehabil. Res.* **1998**, *21* (2), 143.
1142   (6)   Brandstater, M. E.; de Bruin, H.; Gowland, C.; Clark, B. M. Hemiplegic Gait: Analysis of Temporal
1143   Variables. *Arch. Phys. Med. Rehabil.* **1983**, *64* (12), 583–587.
1144   (7)   Chen, G.; Patten, C.; Kothari, D. H.; Zajac, F. E. Gait Deviations Associated with Post-Stroke
1145   Hemiparesis: Improvement during Treadmill Walking Using Weight Support, Speed, Support

Stiffness, and Handrail Hold. *Gait Posture* **2005**, *22* (1), 57–62. https://doi.org/10.1016/j.gaitpost.2004.06.008.

(8)   Olney, S. J.; Monga, T. N.; Costigan, P. A. Mechanical Energy of Walking of Stroke Patients. *Arch. Phys. Med. Rehabil.* **1986**, *67* (2), 92–98. https://doi.org/10.1016/0003-9993(86)90109-7.

(9)   Rejnö, Å.; Nasic, S.; Bjälkefur, K.; Bertholds, E.; Jood, K. Changes in Functional Outcome over Five Years after Stroke. *Brain Behav.* **2019**, *9* (6), e01300. https://doi.org/10.1002/brb3.1300.

(10) Barbour, K. E. Vital Signs: Prevalence of Doctor-Diagnosed Arthritis and Arthritis-Attributable Activity Limitation — United States, 2013–2015. *MMWR Morb. Mortal. Wkly. Rep.* **2017**, *66*. https://doi.org/10.15585/mmwr.mm6609e1.

(11) Kahlenberg, C. A.; Nwachukwu, B. U.; McLawhorn, A. S.; Cross, M. B.; Cornell, C. N.; Padgett, D. E. Patient Satisfaction after Total Knee Replacement: A Systematic Review. *HSS Journal®* **2018**, *14* (2), 192–201. https://doi.org/10.1007/s11420-018-9614-8.

(12) Muertizha, M.; Cai, X.; Ji, B.; Aimaiti, A.; Cao, L. Factors Contributing to 1-Year Dissatisfaction after Total Knee Arthroplasty: A Nomogram Prediction Model. *J. Orthop. Surg.* **2022**, *17* (1), 367. https://doi.org/10.1186/s13018-022-03205-2.

(13) Bourne, R. B.; Chesworth, B. M.; Davis, A. M.; Mahomed, N. N.; Charron, K. D. J. Patient Satisfaction after Total Knee Arthroplasty: Who Is Satisfied and Who Is Not? *Clin. Orthop.* **2009**, *468* (1), 57. https://doi.org/10.1007/s11999-009-1119-9.

(14) Anakwe, R. E.; Jenkins, P. J.; Moran, M. Predicting Dissatisfaction After Total Hip Arthroplasty: A Study of 850 Patients. *J. Arthroplasty* **2011**, *26* (2), 209–213. https://doi.org/10.1016/j.arth.2010.03.013.

(15) Tilbury, C.; Haanstra, T. M.; Leichtenberg, C. S.; Verdegaal, S. H. M.; Ostelo, R. W.; Vet, H. C. W. de; Nelissen, R. G. H. H.; Vlieland, T. P. M. V. Unfulfilled Expectations After Total Hip and Knee Arthroplasty Surgery: There Is a Need for Better Preoperative Patient Information and Education. *J. Arthroplasty* **2016**, *31* (10), 2139–2145. https://doi.org/10.1016/j.arth.2016.02.061.

(16) Kim, M. S.; Koh, I. J.; Kim, C. K.; Choi, K. Y.; Yang, J. S.; In, Y. Patient Expectations and Satisfaction After Medial Opening Wedge High Tibial Osteotomy. *J. Arthroplasty* **2020**, *35* (12), 3467–3473. https://doi.org/10.1016/j.arth.2020.06.076.

(17) Stephan-Carlier, A.; Facione, J.; Speyer, E.; Rumilly, E.; Paysant, J. Quality of Life and Satisfaction after Multilevel Surgery in Cerebral Palsy: Confronting the Experience of Children and Their Parents. *Ann. Phys. Rehabil. Med.* **2014**, *57* (9–10), 640–652. https://doi.org/10.1016/j.rehab.2014.09.012.

(18) Blumetti, F. C.; Wu, J. C. N.; Bau, K. V.; Martin, B.; Hobson, S. A.; Axt, M. W.; Selber, P. Orthopedic Surgery and Mobility Goals for Children with Cerebral Palsy GMFCS Level IV: What Are We Setting out to Achieve? *J. Child. Orthop.* **2012**, *6* (6), 485–490. https://doi.org/10.1007/s11832-012-0454-7.

(19) Schwartz, M. H.; Ries, A. J.; Georgiadis, A. G.; Kainz, H. Demonstrating the Utility of Instrumented Gait Analysis in the Treatment of Children with Cerebral Palsy. *PLOS ONE* **2024**, *19* (4), e0301230. https://doi.org/10.1371/journal.pone.0301230.

(20) DadeMatthews, O. O.; Roper, J. A.; Vazquez, A.; Shannon, D. M.; Sefton, J. M. Prosthetic Device and Service Satisfaction, Quality of Life, and Functional Performance in Lower Limb Prosthesis Clients. *Prosthet. Orthot. Int.* **2024**, *48* (4), 422–430. https://doi.org/10.1097/PXR.0000000000000285.

(21) Datta, D.; Selvarajah, K.; Davey, N. Functional Outcome of Patients with Proximal Upper Limb Deficiency--Acquired and Congenital. *Clin. Rehabil.* **2004**, *18* (2), 172–177. https://doi.org/10.1191/0269215504cr716oa.

(22) *The designer changing the way aircraft are built*. https://www.bbc.com/future/article/20181129-the-ai-transforming-the-way-aircraft-are-built (accessed 2024-09-13).

1194   (23)   *SpaceX Is Using These Simulations to Design the Rocket That'll Take Us to Mars*.
1195   https://www.vice.com/en/article/spacex-is-using-these-simulations-to-design-the-rocket-thatll-
1196   take-us-to-mars/ (accessed 2024-09-13).
1197   (24)   *A brief history of computing in Formula 1*. https://www.mclaren.com/racing/team/a-brief-
1198   history-of-computing-in-f1-1052199/ (accessed 2024-09-13).
1199   (25)   *The America's Cup: nerves, skill, and computer design | PCWorld*.
1200   https://www.pcworld.com/article/447831/the-americas-cup-nerves-skill-and-a-lot-of-
1201   computers.html (accessed 2024-09-13).
1202   (26)   *Planning and Design of Engineering Systems | Graeme Dandy, David Walke*.
1203   https://www.taylorfrancis.com/books/mono/10.1201/9781351228121/planning-design-
1204   engineering-systems-graeme-dandy-trevor-daniell-robert-warner-bernadette-foley-graeme-
1205   dandy-david-walker-trevor-daniell-robert-warner (accessed 2024-09-13).
1206   (27)   López Gualdrón, C.-I.; Bravo Ibarra, E.-R.; Murillo Bohórquez, A.-P.; Garnica Bohórquez, I. Present
1207   and Future for Technologies to Develop Patient-Specific Medical Devices: A Systematic Review
1208   Approach. *Med. Devices Auckl. NZ* **2019**, *12*, 253–273. https://doi.org/10.2147/MDER.S215947.
1209   (28)   U, V.; Mehrotra, D.; Howlader, D.; Singh, P. K.; Gupta, S. Patient Specific Three-Dimensional
1210   Implant for Reconstruction of Complex Mandibular Defect. *J. Craniofac. Surg.* **2019**, *30* (4), e308–
1211   e311. https://doi.org/10.1097/SCS.0000000000005228.
1212   (29)   Sutradhar, A.; Park, J.; Carrau, D.; Miller, M. J. Experimental Validation of 3D Printed Patient-
1213   Specific Implants Using Digital Image Correlation and Finite Element Analysis. *Comput. Biol. Med.*
1214   **2014**, *52*, 8–17. https://doi.org/10.1016/j.compbiomed.2014.06.002.
1215   (30)   Pinheiro, M.; Alves, J. L. The Feasibility of a Custom-Made Endoprosthesis in Mandibular
1216   Reconstruction: Implant Design and Finite Element Analysis. *J. Cranio-Maxillofac. Surg.* **2015**, *43*
1217   (10), 2116–2128. https://doi.org/10.1016/j.jcms.2015.10.004.
1218   (31)   *Transforming the Diagnosis and Management of Coronary Artery Disease*.
1219   https://www.heartflow.com/. https://www.heartflow.com/ (accessed 2024-09-13).
1220   (32)   Hlatky, M. A.; De Bruyne, B.; Pontone, G.; Patel, M. R.; Norgaard, B. L.; Byrne, R. A.; Curzen, N.;
1221   Purcell, I.; Gutberlet, M.; Rioufol, G.; Hink, U.; Schuchlenz, H. W.; Feuchtner, G.; Gilard, M.;
1222   Andreini, D.; Jensen, J. M.; Hadamitzky, M.; Wilk, A.; Wang, F.; Rogers, C.; Douglas, P. S.;
1223   PLATFORM Investigators. Quality-of-Life and Economic Outcomes of Assessing Fractional Flow
1224   Reserve With Computed Tomography Angiography: PLATFORM. *J. Am. Coll. Cardiol.* **2015**, *66*
1225   (21), 2315–2323. https://doi.org/10.1016/j.jacc.2015.09.051.
1226   (33)   Douglas, P. S.; Pontone, G.; Hlatky, M. A.; Patel, M. R.; Norgaard, B. L.; Byrne, R. A.; Curzen, N.;
1227   Purcell, I.; Gutberlet, M.; Rioufol, G.; Hink, U.; Schuchlenz, H. W.; Feuchtner, G.; Gilard, M.;
1228   Andreini, D.; Jensen, J. M.; Hadamitzky, M.; Chiswell, K.; Cyr, D.; Wilk, A.; Wang, F.; Rogers, C.; De
1229   Bruyne, B. Clinical Outcomes of Fractional Flow Reserve by Computed Tomographic Angiography-
1230   Guided Diagnostic Strategies vs. Usual Care in Patients with Suspected Coronary Artery Disease:
1231   The Prospective Longitudinal Trial of FFRCT: Outcome and Resource Impacts Study. *Eur. Heart J.*
1232   **2015**, *36* (47), 3359–3367. https://doi.org/10.1093/eurheartj/ehv444.
1233   (34)   Fregly, B. J. A Conceptual Blueprint for Making Neuromusculoskeletal Models Clinically Useful.
1234   *Appl. Sci.* **2021**, *11* (5), 2037. https://doi.org/10.3390/app11052037.
1235   (35)   Umberger, B. R.; Miller, R. H. Optimal Control Modeling of Human Movement. In *Handbook of*
1236   *Human Motion*; Müller, B., Wolf, S. I., Brueggemann, G.-P., Deng, Z., McIntosh, A., Miller, F.,
1237   Selbie, W. S., Eds.; Springer International Publishing: Cham, 2017; pp 1–22.
1238   https://doi.org/10.1007/978-3-319-30808-1_177-1.
1239   (36)   Lee, L.-F.; Umberger, B. R. Generating Optimal Control Simulations of Musculoskeletal Movement
1240   Using OpenSim and MATLAB. *PeerJ* **2016**, *4*, e1638. https://doi.org/10.7717/peerj.1638.
1241   (37)   Porsa, S.; Lin, Y.-C.; Pandy, M. G. Direct Methods for Predicting Movement Biomechanics Based

Upon Optimal Control Theory with Implementation in OpenSim. *Ann. Biomed. Eng.* **2016**, *44* (8), 2542–2557. https://doi.org/10.1007/s10439-015-1538-6.

(38) Pandy, M. G.; Zajac, F. E.; Sim, E.; Levine, W. S. An Optimal Control Model for Maximum-Height Human Jumping. *J. Biomech.* **1990**, *23* (12), 1185–1198. https://doi.org/10.1016/0021-9290(90)90376-E.

(39) van den Bogert, A. J.; Hupperets, M.; Schlarb, H.; Krabbe, B. Predictive Musculoskeletal Simulation Using Optimal Control: Effects of Added Limb Mass on Energy Cost and Kinematics of Walking and Running. *Proc. Inst. Mech. Eng. Part P J. Sports Eng. Technol.* **2012**, *226* (2), 123–133. https://doi.org/10.1177/1754337112440644.

(40) Rohani, F.; Richter, H.; Bogert, A. J. van den. Optimal Design and Control of an Electromechanical Transfemoral Prosthesis with Energy Regeneration. *PLOS ONE* **2017**, *12* (11), e0188266. https://doi.org/10.1371/journal.pone.0188266.

(41) Meyer, A. J.; Eskinazi, I.; Jackson, J. N.; Rao, A. V.; Patten, C.; Fregly, B. J. Muscle Synergies Facilitate Computational Prediction of Subject-Specific Walking Motions. *Front. Bioeng. Biotechnol.* **2016**, *4*. https://doi.org/10.3389/fbioe.2016.00077.

(42) Dorn, T. W.; Wang, J. M.; Hicks, J. L.; Delp, S. L. Predictive Simulation Generates Human Adaptations during Loaded and Inclined Walking. *PLOS ONE* **2015**, *10* (4), e0121407. https://doi.org/10.1371/journal.pone.0121407.

(43) Ong, C. F.; Geijtenbeek, T.; Hicks, J. L.; Delp, S. L. Predicting Gait Adaptations Due to Ankle Plantarflexor Muscle Weakness and Contracture Using Physics-Based Musculoskeletal Simulations. *PLOS Comput. Biol.* **2019**, *15* (10), e1006993. https://doi.org/10.1371/journal.pcbi.1006993.

(44) Miller, R. H.; Esterson, A. Y.; Shim, J. K. Joint Contact Forces When Minimizing the External Knee Adduction Moment by Gait Modification: A Computer Simulation Study. *The Knee* **2015**, *22* (6), 481–489. https://doi.org/10.1016/j.knee.2015.06.014.

(45) Miller, R. H. A Comparison of Muscle Energy Models for Simulating Human Walking in Three Dimensions. *J. Biomech.* **2014**, *47* (6), 1373–1381. https://doi.org/10.1016/j.jbiomech.2014.01.049.

(46) McGowan, C. P.; Neptune, R. R.; Clark, D. J.; Kautz, S. A. Modular Control of Human Walking: Adaptations to Altered Mechanical Demands. *J. Biomech.* **2010**, *43* (3), 412–419. https://doi.org/10.1016/j.jbiomech.2009.10.009.

(47) Allen, J. L.; Neptune, R. R. Three-Dimensional Modular Control of Human Walking. *J. Biomech.* **2012**, *45* (12), 2157–2163. https://doi.org/10.1016/j.jbiomech.2012.05.037.

(48) Dembia, C. L.; Bianco, N. A.; Falisse, A.; Hicks, J. L.; Delp, S. L. OpenSim Moco: Musculoskeletal Optimal Control. *PLOS Comput. Biol.* **2020**, *16* (12), e1008493. https://doi.org/10.1371/journal.pcbi.1008493.

(49) Delp, S. L.; Anderson, F. C.; Arnold, A. S.; Loan, P.; Habib, A.; John, C. T.; Guendelman, E.; Thelen, D. G. OpenSim: Open-Source Software to Create and Analyze Dynamic Simulations of Movement. *IEEE Trans. Biomed. Eng.* **2007**, *54* (11), 1940–1950. https://doi.org/10.1109/TBME.2007.901024.

(50) Seth, A.; Hicks, J. L.; Uchida, T. K.; Habib, A.; Dembia, C. L.; Dunne, J. J.; Ong, C. F.; DeMers, M. S.; Rajagopal, A.; Millard, M.; Hamner, S. R.; Arnold, E. M.; Yong, J. R.; Lakshmikanth, S. K.; Sherman, M. A.; Ku, J. P.; Delp, S. L. OpenSim: Simulating Musculoskeletal Dynamics and Neuromuscular Control to Study Human and Animal Movement. *PLOS Comput. Biol.* **2018**, *14* (7), e1006223. https://doi.org/10.1371/journal.pcbi.1006223.

(51) Pitto, L.; Kainz, H.; Falisse, A.; Wesseling, M.; Van Rossom, S.; Hoang, H.; Papageorgiou, E.; Hallemans, A.; Desloovere, K.; Molenaers, G.; Van Campenhout, A.; De Groote, F.; Jonkers, I. SimCP: A Simulation Platform to Predict Gait Performance Following Orthopedic Intervention in Children With Cerebral Palsy. *Front. Neurorobotics* **2019**, *13*.

1290   https://doi.org/10.3389/fnbot.2019.00054.

1291   (52) Valente, G.; Crimi, G.; Vanella, N.; Schileo, E.; Taddei, F. nmsBuilder: Freeware to Create Subject-
1292   Specific Musculoskeletal Models for OpenSim. *Comput. Methods Programs Biomed.* **2017**, *152*,
1293   85–92. https://doi.org/10.1016/j.cmpb.2017.09.012.

1294   (53) Zhang, J.; Sorby, H.; Clement, J.; Thomas, C. D. L.; Hunter, P.; Nielsen, P.; Lloyd, D.; Taylor, M.;
1295   Besier, T. The MAP Client: User-Friendly Musculoskeletal Modelling Workflows. In *Biomedical*
1296   *Simulation*; Bello, F., Cotin, S., Eds.; Springer International Publishing: Cham, 2014; pp 182–192.
1297   https://doi.org/10.1007/978-3-319-12057-7_21.

1298   (54) Veerkamp, K.; Kainz, H.; Killen, B. A.; Jónasdóttir, H.; van der Krogt, M. M. Torsion Tool: An
1299   Automated Tool for Personalising Femoral and Tibial Geometries in OpenSim Musculoskeletal
1300   Models. *J. Biomech.* **2021**, *125*, 110589. https://doi.org/10.1016/j.jbiomech.2021.110589.

1301   (55) Modenese, L.; Barzan, M.; Carty, C. P. Dependency of Lower Limb Joint Reaction Forces on
1302   Femoral Version. *Gait Posture* **2021**, *88*, 318–321.
1303   https://doi.org/10.1016/j.gaitpost.2021.06.014.

1304   (56) Werling, K.; Bianco, N. A.; Raitor, M.; Stingel, J.; Hicks, J. L.; Collins, S. H.; Delp, S. L.; Liu, C. K.
1305   AddBiomechanics: Automating Model Scaling, Inverse Kinematics, and Inverse Dynamics from
1306   Human Motion Data through Sequential Optimization. *PLOS ONE* **2023**, *18* (11), e0295152.
1307   https://doi.org/10.1371/journal.pone.0295152.

1308   (57) Kewley, A.; Beesel, J.; Seth, A. OpenSim Creator, 2025.
1309   https://doi.org/10.5281/zenodo.14755649.

1310   (58) Di Pietro, A.; Bersani, A.; Curreli, C.; Di Puccio, F. AST: An OpenSim-Based Tool for the Automatic
1311   Scaling of Generic Musculoskeletal Models. *Comput. Biol. Med.* **2024**, *175*, 108524.
1312   https://doi.org/10.1016/j.compbiomed.2024.108524.

1313   (59) van den Bogert, A. J.; Blana, D.; Heinrich, D. Implicit Methods for Efficient Musculoskeletal
1314   Simulation and Optimal Control. *Procedia IUTAM* **2011**, *2* (2011), 297–316.
1315   https://doi.org/10.1016/j.piutam.2011.04.027.

1316   (60) Patterson, M. A.; Rao, A. V. GPOPS-II: A MATLAB Software for Solving Multiple-Phase Optimal
1317   Control Problems Using Hp-Adaptive Gaussian Quadrature Collocation Methods and Sparse
1318   Nonlinear Programming. *ACM Trans Math Softw* **2014**, *41* (1), 1:1-1:37.
1319   https://doi.org/10.1145/2558904.

1320   (61) De Groote, F.; Kinney, A. L.; Rao, A. V.; Fregly, B. J. Evaluation of Direct Collocation Optimal
1321   Control Problem Formulations for Solving the Muscle Redundancy Problem. *Ann. Biomed. Eng.*
1322   **2016**, *44* (10), 2922–2936. https://doi.org/10.1007/s10439-016-1591-9.

1323   (62) Febrer-Nafría, M.; Pallarès-López, R.; Fregly, B. J.; Font-Llagunes, J. M. Comparison of Different
1324   Optimal Control Formulations for Generating Dynamically Consistent Crutch Walking Simulations
1325   Using a Torque-Driven Model. *Mech. Mach. Theory* **2020**, *154*, 104031.
1326   https://doi.org/10.1016/j.mechmachtheory.2020.104031.

1327   (63) Butler, D. Translational Research: Crossing the Valley of Death. *Nature* **2008**, *453* (7197), 840–
1328   842. https://doi.org/10.1038/453840a.

1329   (64) Jørgensen, J. T. Twenty Years with Personalized Medicine: Past, Present, and Future of
1330   Individualized Pharmacotherapy. *The Oncologist* **2019**, *24* (7), e432–e440.
1331   https://doi.org/10.1634/theoncologist.2019-0054.

1332   (65) Rassmussen J; Vondrak V; Damsgaard M; de Zee M; Christensen ST. The AnyBody Project –
1333   Computer Analysis of the Human Body. *Comput. Anal. Hum. Body* **2002**, No. Biomechanics of
1334   Man, 270–274.

1335   (66) Wächter, A.; Biegler, L. T. On the Implementation of an Interior-Point Filter Line-Search Algorithm
1336   for Large-Scale Nonlinear Programming. *Math. Program.* **2006**, *106* (1), 25–57.
1337   https://doi.org/10.1007/s10107-004-0559-y.

(67) Sauder, N. R.; Meyer, A. J.; Allen, J. L.; Ting, L. H.; Kesar, T. M.; Fregly, B. J. Computational Design of FastFES Treatment to Improve Propulsive Force Symmetry During Post-Stroke Gait: A Feasibility Study. *Front. Neurorobotics* **2019**, *13*, 80. https://doi.org/10.3389/fnbot.2019.00080.

(68) Vega, M. M.; Li, G.; Shourijeh, M. S.; Ao, D.; Weinschenk, R. C.; Patten, C.; Font-Llagunes, J. M.; Lewis, V. O.; Fregly, B. J. Computational Evaluation of Psoas Muscle Influence on Walking Function Following Internal Hemipelvectomy with Reconstruction. *Front. Bioeng. Biotechnol.* **2022**, *10*, 855870. https://doi.org/10.3389/fbioe.2022.855870.

(69) McMorland, A. J. C.; Runnalls, K. D.; Byblow, W. D. A Neuroanatomical Framework for Upper Limb Synergies after Stroke. *Front. Hum. Neurosci.* **2015**, *9*. https://doi.org/10.3389/fnhum.2015.00082.

(70) Akhras, M. A.; Bortoletto, R.; Madehkhaksar, F.; Tagliapietra, L. Neural and Musculoskeletal Modeling: Its Role in Neurorehabilitation. In *Emerging Therapies in Neurorehabilitation II*; Pons, J. L., Raya, R., González, J., Eds.; Springer International Publishing: Cham, 2016; pp 109–143. https://doi.org/10.1007/978-3-319-24901-8_5.

(71) Meyer, A. J.; Patten, C.; Fregly, B. J. Lower Extremity EMG-Driven Modeling of Walking with Automated Adjustment of Musculoskeletal Geometry. *PLOS ONE* **2017**, *12* (7), e0179698. https://doi.org/10.1371/journal.pone.0179698.

(72) Reinbolt, J. A.; Haftka, R. T.; Chmielewski, T. L.; Fregly, B. J. Are Patient-Specific Joint and Inertial Parameters Necessary for Accurate Inverse Dynamics Analyses of Gait? *IEEE Trans. Biomed. Eng.* **2007**, *54* (5), 782–793. https://doi.org/10.1109/TBME.2006.889187.

(73) Serrancolí, G.; Kinney, A. L.; Fregly, B. J.; Font-Llagunes, J. M. Neuromusculoskeletal Model Calibration Significantly Affects Predicted Knee Contact Forces for Walking. *J. Biomech. Eng.* **2016**, *138* (8), 0810011–08100111. https://doi.org/10.1115/1.4033673.

(74) Żuk, M.; Syczewska, M.; Pezowicz, C. Influence of Uncertainty in Selected Musculoskeletal Model Parameters on Muscle Forces Estimated in Inverse Dynamics-Based Static Optimization and Hybrid Approach. *J. Biomech. Eng.* **2018**, *140* (121001). https://doi.org/10.1115/1.4040943.

(75) Lloyd, D. G.; Besier, T. F. An EMG-Driven Musculoskeletal Model to Estimate Muscle Forces and Knee Joint Moments in Vivo. *J. Biomech.* **2003**, *36* (6), 765–776. https://doi.org/10.1016/s0021-9290(03)00010-1.

(76) Manal, K.; Buchanan, T. S. Use of an EMG-Driven Biomechanical Model to Study Virtual Injuries. *Med. Sci. Sports Exerc.* **2005**, *37* (11), 1917–1923. https://doi.org/10.1249/01.mss.0000176685.35442.6b.

(77) Moissenet, F.; Modenese, L.; Dumas, R. Alterations of Musculoskeletal Models for a More Accurate Estimation of Lower Limb Joint Contact Forces during Normal Gait: A Systematic Review. *J. Biomech.* **2017**, *63*, 8–20. https://doi.org/10.1016/j.jbiomech.2017.08.025.

(78) Arones, M. M.; Shourijeh, M. S.; Patten, C.; Fregly, B. J. Musculoskeletal Model Personalization Affects Metabolic Cost Estimates for Walking. *Front. Bioeng. Biotechnol.* **2020**, *8*, 588925. https://doi.org/10.3389/fbioe.2020.588925.

(79) Jackson, J. N.; Hass, C. J.; Fregly, B. J. Development of a Subject-Specific Foot-Ground Contact Model for Walking. *J. Biomech. Eng.* **2016**, *138* (9), 0910021–09100212. https://doi.org/10.1115/1.4034060.

(80) Nguyen, V. Q.; Johnson, R. T.; Sup, F. C.; Umberger, B. R. Bilevel Optimization for Cost Function Determination in Dynamic Simulation of Human Gait. *IEEE Trans. Neural Syst. Rehabil. Eng. Publ. IEEE Eng. Med. Biol. Soc.* **2019**, *27* (7), 1426–1435. https://doi.org/10.1109/TNSRE.2019.2922942.

(81) Kuska, E. C.; Steele, K. M. Does Crouch Alter the Effects of Neuromuscular Impairments on Gait? A Simulation Study. *J. Biomech.* **2024**, *165*, 112015. https://doi.org/10.1016/j.jbiomech.2024.112015.

(82) Pariser, K. M.; Higginson, J. S. Development and Validation of a Framework for Predictive

1386   Simulation of Treadmill Gait. *J. Biomech. Eng.* **2022**, *144* (11), 114505.
1387   https://doi.org/10.1115/1.4054867.
1388 (83) Falisse, A.; Serrancolí, G.; Dembia, C. L.; Gillis, J.; Jonkers, I.; De Groote, F. Rapid Predictive
1389   Simulations with Complex Musculoskeletal Models Suggest That Diverse Healthy and Pathological
1390   Human Gaits Can Emerge from Similar Control Strategies. *J. R. Soc. Interface* **2019**, *16* (157),
1391   20190402. https://doi.org/10.1098/rsif.2019.0402.
1392 (84) Dorschky, E.; Nitschke, M.; Seifer, A.-K.; van den Bogert, A. J.; Eskofier, B. M. Estimation of Gait
1393   Kinematics and Kinetics from Inertial Sensor Data Using Optimal Control of Musculoskeletal
1394   Models. *J. Biomech.* **2019**, *95*, 109278. https://doi.org/10.1016/j.jbiomech.2019.07.022.
1395 (85) Ackermann, M.; van den Bogert, A. J. Optimality Principles for Model-Based Prediction of Human
1396   Gait. *J. Biomech.* **2010**, *43* (6), 1055–1060. https://doi.org/10.1016/j.jbiomech.2009.12.012.
1397 (86) Johnson, R. T.; Bianco, N. A.; Finley, J. M. Patterns of Asymmetry and Energy Cost Generated from
1398   Predictive Simulations of Hemiparetic Gait. *PLoS Comput. Biol.* **2022**, *18* (9), e1010466.
1399   https://doi.org/10.1371/journal.pcbi.1010466.
1400 (87) Miller, R. H.; Russell Esposito, E. Transtibial Limb Loss Does Not Increase Metabolic Cost in Three-
1401   Dimensional Computer Simulations of Human Walking. *PeerJ* **2021**, *9*, e11960.
1402   https://doi.org/10.7717/peerj.11960.
1403 (88) Weng, J.; Hashemi, E.; Arami, A. Adaptive Reference Inverse Optimal Control for Natural Walking
1404   With Musculoskeletal Models. *IEEE Trans. Neural Syst. Rehabil. Eng.* **2022**, *30*, 1567–1575.
1405   https://doi.org/10.1109/TNSRE.2022.3180690.
1406 (89) Tresch, M. C.; Saltiel, P.; Bizzi, E. The Construction of Movement by the Spinal Cord. *Nat.
1407   Neurosci.* **1999**, *2* (2), 162–167. https://doi.org/10.1038/5721.
1408 (90) Lee, D.; Seung, H. Algorithms for Non-Negative Matrix Factorization. *Adv Neural Inf. Process Syst*
1409   **2001**, *13*.
1410 (91) Ivanenko, Y. P.; Poppele, R. E.; Lacquaniti, F. Five Basic Muscle Activation Patterns Account for
1411   Muscle Activity during Human Locomotion. *J. Physiol.* **2004**, *556* (Pt 1), 267–282.
1412   https://doi.org/10.1113/jphysiol.2003.057174.
1413 (92) Cheung, V. C. K.; Piron, L.; Agostini, M.; Silvoni, S.; Turolla, A.; Bizzi, E. Stability of Muscle
1414   Synergies for Voluntary Actions after Cortical Stroke in Humans. *Proc. Natl. Acad. Sci. U. S. A.*
1415   **2009**, *106* (46), 19563. https://doi.org/10.1073/pnas.0910114106.
1416 (93) Clark, D. J.; Ting, L. H.; Zajac, F. E.; Neptune, R. R.; Kautz, S. A. Merging of Healthy Motor Modules
1417   Predicts Reduced Locomotor Performance and Muscle Coordination Complexity Post-Stroke. *J.
1418   Neurophysiol.* **2010**, *103* (2), 844–857. https://doi.org/10.1152/jn.00825.2009.
1419 (94) Gizzi, L.; Nielsen, J. F.; Felici, F.; Ivanenko, Y. P.; Farina, D. Impulses of Activation but Not Motor
1420   Modules Are Preserved in the Locomotion of Subacute Stroke Patients. *J. Neurophysiol.* **2011**, *106*
1421   (1), 202–210. https://doi.org/10.1152/jn.00727.2010.
1422 (95) Routson, R. L.; Clark, D. J.; Bowden, M. G.; Kautz, S. A.; Neptune, R. R. The Influence of Locomotor
1423   Rehabilitation on Module Quality and Post-Stroke Hemiparetic Walking Performance. *Gait
1424   Posture* **2013**, *38* (3), 511–517. https://doi.org/10.1016/j.gaitpost.2013.01.020.
1425 (96) Roh, J.; Rymer, W. Z.; Perreault, E. J.; Yoo, S. B.; Beer, R. F. Alterations in Upper Limb Muscle
1426   Synergy Structure in Chronic Stroke Survivors. *J. Neurophysiol.* **2013**, *109* (3), 768–781.
1427   https://doi.org/10.1152/jn.00670.2012.
1428 (97) Pitto, L.; Rossom, S. van; Desloovere, K.; Molenaers, G.; Huenaerts, C.; Groote, F. D.; Jonkers, I.
1429   Pre-Treatment EMG Can Be Used to Model Post-Treatment Muscle Coordination during Walking
1430   in Children with Cerebral Palsy. *PLOS ONE* **2020**, *15* (2), e0228851.
1431   https://doi.org/10.1371/journal.pone.0228851.
1432 (98) Rabbi, M. F.; Pizzolato, C.; Lloyd, D. G.; Carty, C. P.; Devaprakash, D.; Diamond, L. E. Non-Negative
1433   Matrix Factorisation Is the Most Appropriate Method for Extraction of Muscle Synergies in

1434   Walking and Running. *Sci. Rep.* **2020**, *10* (1), 8266. https://doi.org/10.1038/s41598-020-65257-w.

1435   (99)   Rajagopal, A.; Dembia, C. L.; DeMers, M. S.; Delp, D. D.; Hicks, J. L.; Delp, S. L. Full-Body
1436   Musculoskeletal Model for Muscle-Driven Simulation of Human Gait. *IEEE Trans. Biomed. Eng.*
1437   **2016**, *63* (10), 2068–2079. https://doi.org/10.1109/TBME.2016.2586891.

1438   (100)   van den Bogert, A. J.; Smith, G. D.; Nigg, B. M. In Vivo Determination of the Anatomical Axes of
1439   the Ankle Joint Complex: An Optimization Approach. *J. Biomech.* **1994**, *27* (12), 1477–1488.
1440   https://doi.org/10.1016/0021-9290(94)90197-x.

1441   (101)   Reinbolt, J. A.; Schutte, J. F.; Fregly, B. J.; Koh, B. I.; Haftka, R. T.; George, A. D.; Mitchell, K. H.
1442   Determination of Patient-Specific Multi-Joint Kinematic Models through Two-Level Optimization.
1443   *J. Biomech.* **2005**, *38* (3), 621–626. https://doi.org/10.1016/j.jbiomech.2004.03.031.

1444   (102)   Price, M. A.; LaPrè, A. K.; Johnson, R. T.; Umberger, B. R.; Sup IV, F. C. A Model-Based Motion
1445   Capture Marker Location Refinement Approach Using Inverse Kinematics from Dynamic Trials.
1446   *Int. J. Numer. Methods Biomed. Eng.* **2020**, *36* (1), e3283. https://doi.org/10.1002/cnm.3283.

1447   (103)   Xu, D.; Carlton, L. G.; Rosengren, K. S. Anticipatory Postural Adjustments for Altering Direction
1448   during Walking. *J. Mot. Behav.* **2004**, *36* (3), 316–326. https://doi.org/10.3200/JMBR.36.3.316-
1449   326.

1450   (104)   Bell, A. L.; Pedersen, D. R.; Brand, R. A. A Comparison of the Accuracy of Several Hip Center
1451   Location Prediction Methods. *J. Biomech.* **1990**, *23* (6), 617–621. https://doi.org/10.1016/0021-
1452   9290(90)90054-7.

1453   (105)   Leardini, A.; Cappozzo, A.; Catani, F.; Toksvig-Larsen, S.; Petitto, A.; Sforza, V.; Cassanelli, G.;
1454   Giannini, S. Validation of a Functional Method for the Estimation of Hip Joint Centre Location. *J.*
1455   *Biomech.* **1999**, *32* (1), 99–103. https://doi.org/10.1016/S0021-9290(98)00148-1.

1456   (106)   Charlton, I. W.; Tate, P.; Smyth, P.; Roren, L. Repeatability of an Optimised Lower Body Model.
1457   *Gait Posture* **2004**, *20* (2), 213–221. https://doi.org/10.1016/j.gaitpost.2003.09.004.

1458   (107)   Chèze, L.; Fregly, B. J.; Dimnet, J. Determination of Joint Functional Axes from Noisy Marker Data
1459   Using the Finite Helical Axis. *Hum. Mov. Sci.* **1998**, *17* (1), 1–15. https://doi.org/10.1016/S0167-
1460   9457(97)00018-3.

1461   (108)   Sartori, M.; Reggiani, M.; Farina, D.; Lloyd, D. G. EMG-Driven Forward-Dynamic Estimation of
1462   Muscle Force and Joint Moment about Multiple Degrees of Freedom in the Human Lower
1463   Extremity. *PLOS ONE* **2012**, *7* (12), e52618. https://doi.org/10.1371/journal.pone.0052618.

1464   (109)   Pizzolato, C.; Lloyd, D. G.; Sartori, M.; Ceseracciu, E.; Besier, T. F.; Fregly, B. J.; Reggiani, M.
1465   CEINMS: A Toolbox to Investigate the Influence of Different Neural Control Solutions on the
1466   Prediction of Muscle Excitation and Joint Moments during Dynamic Motor Tasks. *J. Biomech.*
1467   **2015**, *48* (14), 3929–3936. https://doi.org/10.1016/j.jbiomech.2015.09.021.

1468   (110)   De Groote, F.; Van Campen, A.; Jonkers, I.; De Schutter, J. Sensitivity of Dynamic Simulations of
1469   Gait and Dynamometer Experiments to Hill Muscle Model Parameters of Knee Flexors and
1470   Extensors. *J. Biomech.* **2010**, *43* (10), 1876–1883.
1471   https://doi.org/10.1016/j.jbiomech.2010.03.022.

1472   (111)   Anderson, F. C.; Pandy, M. G. Static and Dynamic Optimization Solutions for Gait Are Practically
1473   Equivalent. *J. Biomech.* **2001**, *34* (2), 153–161. https://doi.org/10.1016/S0021-9290(00)00155-X.

1474   (112)   Millard, M.; Uchida, T.; Seth, A.; Delp, S. L. Flexing Computational Muscle: Modeling and
1475   Simulation of Musculotendon Dynamics. *J. Biomech. Eng.* **2013**, *135* (2), 0210051–02100511.
1476   https://doi.org/10.1115/1.4023390.

1477   (113)   Buchanan, T. S.; Lloyd, D. G.; Manal, K.; Besier, T. F. Estimation of Muscle Forces and Joint
1478   Moments Using a Forward-Inverse Dynamics Model. *Med. Sci. Sports Exerc.* **2005**, *37* (11), 1911–
1479   1916. https://doi.org/10.1249/01.mss.0000176684.24008.6f.

1480   (114)   Handsfield, G. G.; Meyer, C. H.; Hart, J. M.; Abel, M. F.; Blemker, S. S. Relationships of 35 Lower
1481   Limb Muscles to Height and Body Mass Quantified Using MRI. *J. Biomech.* **2014**, *47* (3), 631–638.

https://doi.org/10.1016/j.jbiomech.2013.12.002.

(115) Ao, D.; Shourijeh, M. S.; Patten, C.; Fregly, B. J. Evaluation of Synergy Extrapolation for Predicting Unmeasured Muscle Excitations from Measured Muscle Synergies. *Front. Comput. Neurosci.* **2020**, *14*. https://doi.org/10.3389/fncom.2020.588943.

(116) Ao, D.; Vega, M. M.; Shourijeh, M. S.; Patten, C.; Fregly, B. J. EMG-Driven Musculoskeletal Model Calibration with Estimation of Unmeasured Muscle Excitations via Synergy Extrapolation. *Front. Bioeng. Biotechnol.* **2022**, *10*. https://doi.org/10.3389/fbioe.2022.962959.

(117) Di, A.; Benjamin, J. F. Comparison of Synergy Extrapolation and Static Optimization for Estimating Multiple Unmeasured Muscle Activations during Walking. *bioRxiv* **2024**, 2024.03.03.583228. https://doi.org/10.1101/2024.03.03.583228.

(118) Arnold, E. M.; Hamner, S. R.; Seth, A.; Millard, M.; Delp, S. L. How Muscle Fiber Lengths and Velocities Affect Muscle Force Generation as Humans Walk and Run at Different Speeds. *J. Exp. Biol.* **2013**, *216* (11), 2150–2160. https://doi.org/10.1242/jeb.075697.

(119) Gopalakrishnan, A.; Modenese, L.; Phillips, A. T. M. A Novel Computational Framework for Deducing Muscle Synergies from Experimental Joint Moments. *Front. Comput. Neurosci.* **2014**, *8*. https://doi.org/10.3389/fncom.2014.00153.

(120) Shourijeh, M. S.; Fregly, B. J. Muscle Synergies Modify Optimization Estimates of Joint Stiffness During Walking. *J. Biomech. Eng.* **2020**, *142* (1), 011011. https://doi.org/10.1115/1.4044310.

(121) Ivanenko, Y. P.; Cappellini, G.; Dominici, N.; Poppele, R. E.; Lacquaniti, F. Coordination of Locomotion with Voluntary Movements in Humans. *J. Neurosci.* **2005**, *25* (31), 7238–7253. https://doi.org/10.1523/JNEUROSCI.1327-05.2005.

(122) Rodriguez, K. L.; Roemmich, R. T.; Cam, B.; Fregly, B. J.; Hass, C. J. Persons with Parkinson's Disease Exhibit Decreased Neuromuscular Complexity during Gait. *Clin. Neurophysiol.* **2013**, *124* (7), 1390–1397. https://doi.org/10.1016/j.clinph.2013.02.006.

(123) Bhargava, L. J.; Pandy, M. G.; Anderson, F. C. A Phenomenological Model for Estimating Metabolic Energy Consumption in Muscle Contraction. *J. Biomech.* **2004**, *37* (1), 81–88. https://doi.org/10.1016/s0021-9290(03)00239-2.

(124) Roh, J.; Cheung, V. C. K.; Bizzi, E. Modules in the Brain Stem and Spinal Cord Underlying Motor Behaviors. *J. Neurophysiol.* **2011**, *106* (3), 1363–1378. https://doi.org/10.1152/jn.00842.2010.

(125) Cheung, V. C. K.; Piron, L.; Agostini, M.; Silvoni, S.; Turolla, A.; Bizzi, E. Stability of Muscle Synergies for Voluntary Actions after Cortical Stroke in Humans. *Proc. Natl. Acad. Sci.* **2009**, *106* (46), 19563–19568. https://doi.org/10.1073/pnas.0910114106.

(126) Raja, B.; Neptune, R. R.; Kautz, S. A. Coordination of the Non-Paretic Leg During Hemiparetic Gait: Expected and Novel Compensatory Patterns. *Clin. Biomech. Bristol Avon* **2012**, *27* (10), 1023–1030. https://doi.org/10.1016/j.clinbiomech.2012.08.005.

(127) Kautz, S. A.; Patten, C. Interlimb Influences on Paretic Leg Function in Poststroke Hemiparesis. *J. Neurophysiol.* **2005**, *93* (5), 2460–2473. https://doi.org/10.1152/jn.00963.2004.

(128) Sánchez, N.; Acosta, A. M.; López-Rosado, R.; Dewald, J. P. A. Neural Constraints Affect the Ability to Generate Hip Abduction Torques When Combined With Hip Extension or Ankle Plantarflexion in Chronic Hemiparetic Stroke. *Front. Neurol.* **2018**, *9*. https://doi.org/10.3389/fneur.2018.00564.

(129) Pandian, S.; Arya, K. N.; Kumar, D. Does Motor Training of the Nonparetic Side Influences Balance and Function in Chronic Stroke? A Pilot RCT. *Sci. World J.* **2014**, *2014* (1), 769726. https://doi.org/10.1155/2014/769726.

(130) Lim, H.; Madhavan, S. Non-Paretic Leg Movements Can Facilitate Cortical Drive to the Paretic Leg in Individuals Post Stroke with Severe Motor Impairment: Implications for Motor Priming. *Eur. J. Neurosci.* **2023**, *58* (3), 2853–2867. https://doi.org/10.1111/ejn.16069.

(131) Kramer, S.; Johnson, L.; Bernhardt, J.; Cumming, T. Energy Expenditure and Cost During Walking After Stroke: A Systematic Review. *Arch. Phys. Med. Rehabil.* **2016**, *97* (4), 619-632.e1.

1530   https://doi.org/10.1016/j.apmr.2015.11.007.

1531 (132) Hoxie, R. E.; Rubenstein, L. Z.; Hoenig, H.; Gallagher, B. R. The Older Pedestrian. *J. Am. Geriatr.*
1532   *Soc.* **1994**, *42* (4), 444–450. https://doi.org/10.1111/j.1532-5415.1994.tb07496.x.

1533 (133) Perry, J.; Garrett, M.; Gronley, J. K.; Mulroy, S. J. Classification of Walking Handicap in the Stroke
1534   Population. *Stroke* **1995**, *26* (6), 982–989. https://doi.org/10.1161/01.str.26.6.982.

1535 (134) Hug, F.; Turpin, N. A.; Couturier, A.; Dorel, S. Consistency of Muscle Synergies during Pedaling
1536   across Different Mechanical Constraints. *J. Neurophysiol.* **2011**, *106* (1), 91–103.
1537   https://doi.org/10.1152/jn.01096.2010.

1538 (135) Pataky, T. C.; Goulermas, J. Y. Pedobarographic Statistical Parametric Mapping (pSPM): A Pixel-
1539   Level Approach to Foot Pressure Image Analysis. *J. Biomech.* **2008**, *41* (10), 2136–2143.
1540   https://doi.org/10.1016/j.jbiomech.2008.04.034.

1541 (136) Duckworth, T.; Betts, R. P.; Franks, C. I.; Burke, J. The Measurement of Pressures under the Foot.
1542   *Foot Ankle* **1982**, *3* (3), 130–141. https://doi.org/10.1177/107110078200300303.

1543 (137) Li, G.; Ao, D.; Vega, M. M.; Zandiyeh, P.; Chang, S.-H.; Penny, A. N.; Lewis, V. O.; Fregly, B. J.
1544   Changes in Walking Function and Neural Control Following Pelvic Cancer Surgery with
1545   Reconstruction. *Front. Bioeng. Biotechnol.* **2024**, *12*.
1546   https://doi.org/10.3389/fbioe.2024.1389031.

1547 (138) Wirth, M. A.; Kovesi, P. MATLAB as an Introductory Programming Language. *Comput. Appl. Eng.*
1548   *Educ.* **2006**, *14* (1), 20–30. https://doi.org/10.1002/cae.20064.

1549 (139) Vicéns, J. L.; Zamora, B.; Ojados, D. Improvement of the Reflective Learning in Engineering
1550   Education Using MATLAB for Problems Solving. *Comput. Appl. Eng. Educ.* **2016**, *24* (5), 755–764.
1551   https://doi.org/10.1002/cae.21748.

1552 (140) Anderson, F. C.; Pandy, M. G. Static and Dynamic Optimization Solutions for Gait Are Practically
1553   Equivalent. *J. Biomech.* **2001**, *34* (2), 153–161. https://doi.org/10.1016/s0021-9290(00)00155-x.

1554 (141) Suwarganda, E. K.; Diamond, L. E.; Lloyd, D. G.; Besier, T. F.; Zhang, J.; Killen, B. A.; Savage, T. N.;
1555   Saxby, D. J. Minimal Medical Imaging Can Accurately Reconstruct Geometric Bone Models for
1556   Musculoskeletal Models. *PLOS ONE* **2019**, *14* (2), e0205628.
1557   https://doi.org/10.1371/journal.pone.0205628.

1558 (142) Killen, B. A.; Brito da Luz, S.; Lloyd, D. G.; Carleton, A. D.; Zhang, J.; Besier, T. F.; Saxby, D. J.
1559   Automated Creation and Tuning of Personalised Muscle Paths for OpenSim Musculoskeletal
1560   Models of the Knee Joint. *Biomech. Model. Mechanobiol.* **2021**, *20* (2), 521–533.
1561   https://doi.org/10.1007/s10237-020-01398-1.

1562 (143) Kainz, H.; Wesseling, M.; Jonkers, I. Generic Scaled versus Subject-Specific Models for the
1563   Calculation of Musculoskeletal Loading in Cerebral Palsy Gait: Effect of Personalized
1564   Musculoskeletal Geometry Outweighs the Effect of Personalized Neural Control. *Clin. Biomech.*
1565   **2021**, *87*, 105402. https://doi.org/10.1016/j.clinbiomech.2021.105402.

1566 (144) Michaud, F.; Frey-Law, L. A.; Lugrís, U.; Cuadrado, L.; Figueroa-Rodríguez, J.; Cuadrado, J. Applying
1567   a Muscle Fatigue Model When Optimizing Load-Sharing between Muscles for Short-Duration
1568   High-Intensity Exercise: A Preliminary Study. *Front. Physiol.* **2023**, *14*.
1569   https://doi.org/10.3389/fphys.2023.1167748.

1570 (145) Ma, L.; Zhang, W.; Hu, B.; Chablat, D.; Bennis, F.; Guillaume, F. Determination of Subject-Specific
1571   Muscle Fatigue Rates under Static Fatiguing Operations. *Ergonomics* **2013**, *56* (12), 1889–1900.
1572   https://doi.org/10.1080/00140139.2013.851283.

1573 Figure Captions

1574

1575

1576

1577

1578

1579

1580

1581

1582

1583

1584

1585

1586

1587

1588

1589

1590

1591

1592

1593